

Electronic Supplementary Information

Contents

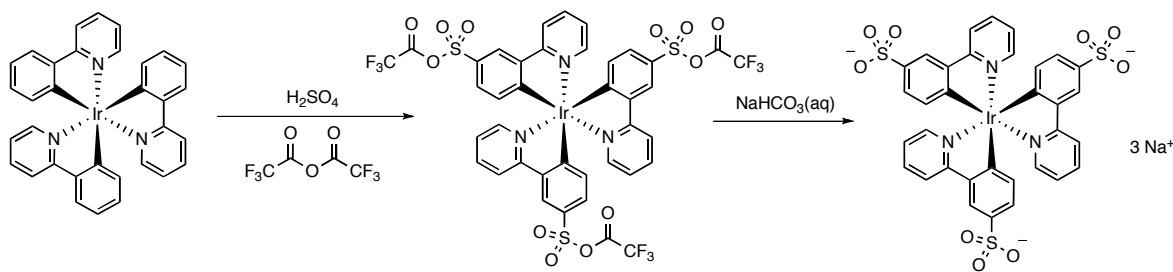
1) General information	S2
2) Synthesis and characterization data for the Na ₃ [Ir(sppy) ₃] photocatalyst	S3
3) Experimental details for the reactions with Na ₃ [Ir(sppy) ₃] / <i>E. coli</i> (MAO-N-9)	S6
3.1 Identification of a suitable photocatalyst for 2-cyclohexyl-1-pyrroline (1a) reduction	S7
3.2 Reduction of 2-cyclohexyl-1-pyrroline (1a) with [Ir]/[MAO-N-9] system	S8
3.3 Kinetic resolution of 2-cyclohexyl-1-pyrrolidine (<i>rac</i> - 2a) with <i>E. coli</i> (MAO-N-9) lysate	S10
3.4 Reduction of 2- <i>n</i> -butyl-1-pyrroline (1b) with [Ir]/[MAO-N-9] system	S12
3.5 Reduction of 2-benzyl-1-pyrroline (1c) with [Ir]/[MAO-N-9] system	S13
3.6 Reduction of 2-cyclohexyl-1-methyl-pyrrolinium iodide (1d) with [Ir]/[MAO-N-9] system	S14
3.7 Reduction of 1-methyl-3,4-dihydroisoquinoline (1e) with [Ir or Ru]/[MAO-N-9] system	S15
4) Monitoring the conversion of 1a to (<i>R</i>)- 2a by chiral GC as a function of time	S24
5) Luminescence quenching experiments with Na ₃ [Ir(sppy) ₃]	S26
6) Cyclic voltammetry of imine substrate 1a and 1e	S30
7) References	S30

1) General information

^1H NMR and ^{13}C NMR spectra were recorded on a Bruker 400 MHz (101 MHz) instrument. ESI mass spectra were acquired on Bruker esquire 3000 plus spectrometer and Bruker maxis 4G QTOF EDI spectrometer for HRMS. Elemental analyses were conducted on a Vario Micro Cube instrument. IR spectra were recorded on an ATR Varian Scimitar 800. Optical absorption spectroscopy was performed using a Cary 5000 instrument from Varian. Steady-state luminescence spectra were measured on a Fluorolog-322 from Horiba Jobin-Yvon. Time-resolved luminescence was measured on a LifeSpec II spectrometer from Edinburgh Instruments with a 405 nm laser as an excitation source. The laser pulse duration was ~ 60 ps and the pulse frequency was 50 kHz. The luminescence decays were recorded using a single photon counting detector. LED lamps from THORLABS with ~ 3 W electric power and ~ 500 mW optical power were used for irradiation of reaction mixtures at 405 and 455 nm. For cyclic voltammetry, a Versastat3-200 potentiostat from Princeton Applied Research was used. A glassy carbon disk electrode served as a working electrode, a silver wire was used as the counter electrode and the reference electrode was a saturated calomel electrode (SCE). Potential sweep rates were 0.1 V/s. *E. coli* cells expressing MAO-N-9 were produced as previously reported.^{S1} *fac*-Ir(ppy)₃ was synthesized according to ref S2. 2-Cyclohexyl-1-pyrroline (**1a**), 2-*n*-butyl-1-pyrroline (**1b**), 2-benzyl-1-pyrroline (**1c**) were prepared according to literature procedures.^{S3} Compound **1d** was synthesized from **1a** by methylation with CH₃I according to ref S4. 1-methyl-3,4-dihydroisoquinoline (**1e**) was purchased from Sigma-Aldrich. The reference racemic amines were prepared from corresponding imines or iminium ions by reduction with NaBH₄ in MeOH.

2) Synthesis and characterization data for the $\text{Na}_3[\text{Ir}(\text{sppy})_3]$ photocatalyst

Procedure for the synthesis of $\text{Na}_3[\text{Ir}(\text{sppy})_3]$: Concentrated sulfuric acid (10 mg, 0.1 mmol) was added to 1 mL trifluoroacetic anhydride (TFAA), the mixture was stirred for ca. 1 h at room temperature until the sulfuric acid was fully dissolved (reacted). A solution of *fac*- $\text{Ir}(\text{ppy})_3$ (20 mg, 0.03 mmol) in dichloromethane (4 mL) was slowly added to the TFAA solution, then the mixture was stirred for additional 12 h. The solvent was evaporated by flushing with nitrogen, and few drops of aqueous sodium bicarbonate solution were added to the solid residue. After removing the solvent, the solid residue was purified by column chromatography on silica gel using water/methanol/acetonitrile (in 1/5/50 volume ratio) as the eluent to afford the desired $\text{Na}_3[\text{Ir}(\text{sppy})_3]$ product (12 mg) as a bright yellow solid in 41% yield.



Scheme S1. Synthesis of $\text{Na}_3[\text{Ir}(\text{sppy})_3]$ through three-fold sulfonation of *fac*- $\text{Ir}(\text{ppy})_3$.

Trisodium *fac*-tris[2-(5'-sulfonatophenyl)pyridine]iridate(III). ^1H NMR (D_2O , 400 MHz) δ 8.15 (d, $J = 1.9$ Hz, 3H), 8.12 (d, $J = 8.2$ Hz, 3H), 7.79 (t, $J = 7.8$ Hz, 3H), 7.63 (d, $J = 5.5$ Hz, 3H), 7.15 (dd, $J = 8.0, 1.9$ Hz, 3H), 7.04 (t, $J = 6.5$ Hz, 3H), 6.84 (d, $J = 8.0$ Hz, 3H); ^{13}C NMR (D_2O , 101 MHz) δ 165.4, 163.8, 147.7, 145.1, 137.7, 136.2, 134.9, 126.0, 123.8, 120.7, 119.8. ESI-MS (m/z) calcd for $\text{C}_{33}\text{H}_{23}\text{IrN}_3\text{O}_9\text{S}_3^-$ [$\text{M}-3\text{Na}^++2\text{H}^+$], $\text{C}_{33}\text{H}_{22}\text{IrN}_3\text{O}_9\text{S}_3^{2-}$ [$\text{M}-3\text{Na}^++\text{H}^+$], $\text{C}_{33}\text{H}_{21}\text{IrN}_3\text{O}_9\text{S}_3^{3-}$ [$\text{M}-3\text{Na}^+$];: 894.0, 446.5, 297.3; found: 893.9, 446.4, 297.1. Anal. calcd. for $\text{C}_{33}\text{H}_{21}\text{IrN}_3\text{Na}_3\text{O}_9\text{S}_3 \cdot 5\text{H}_2\text{O}$: C, 37.72; H, 2.96; N, 4.00; found: C, 37.60; H, 3.26; N, 3.87.

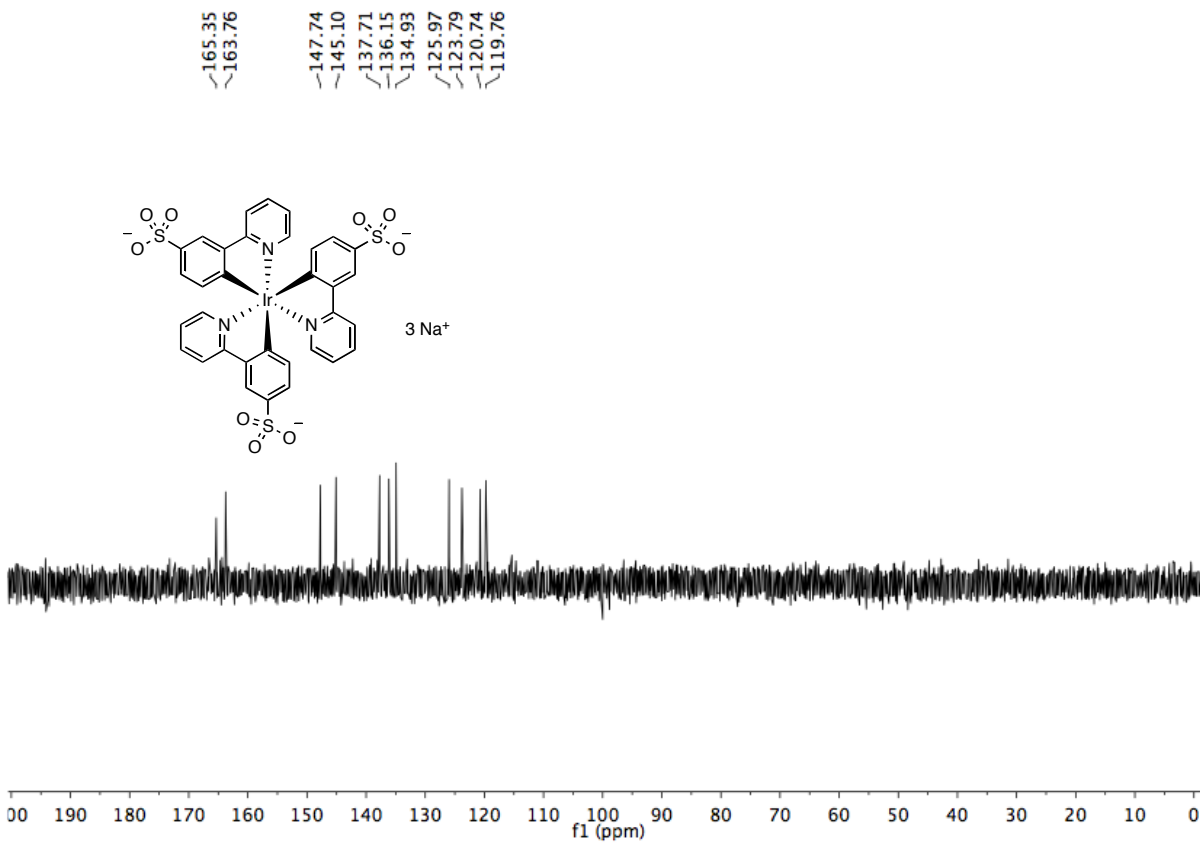
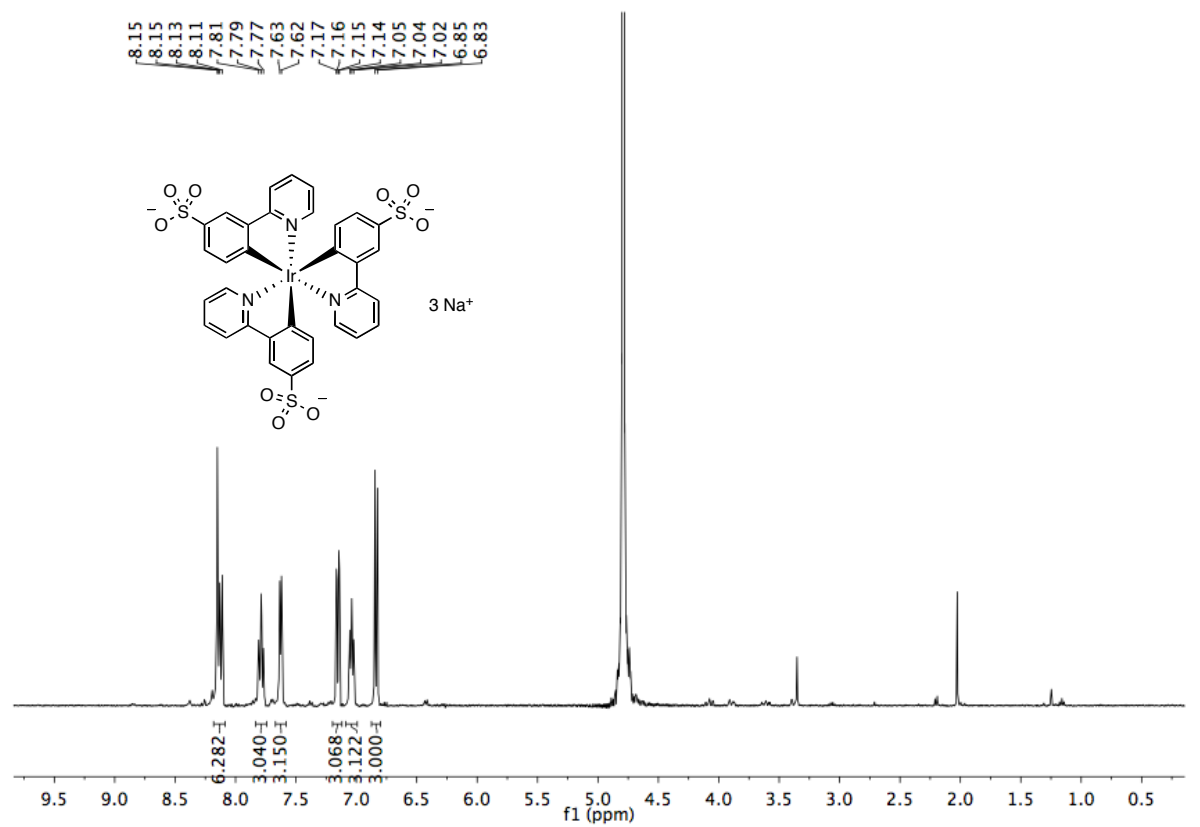


Fig. S1. ^1H and ^{13}C NMR spectra of $\text{Na}_3[\text{Ir}(\text{sppy})_3]$ in D_2O .

Estimation of the excited-state oxidation potential. Using a simplified version of the Rehm-Weller equation (S1),^{S5} the excited-state oxidation potential of the $\text{Na}_3[\text{Ir}(\text{sppy})_3]$ complex was estimated from the ground-state oxidation potential and the energy (E_{0-0}) of the emissive triplet excited state. The latter was estimated from the short-wavelength edge of emission ($\lambda_{10\%}$) where the emission intensity is 10% of that detectable at the emission maximum (λ_{max}).^{S6}

$$E_{\text{ox}}^{0*} = E_{\text{ox}}^0 - E_{0-0} \quad (\text{S1})$$

Table S1. Estimation for triplet state energy and excited state oxidation potential.

$E_{\text{ox}} / \text{V vs. SCE}$	$\lambda_{\text{max}} / \text{nm}$	$\lambda_{10\%} / \text{nm}$	E_{0-0} / eV	$E_{\text{ox}}^* / \text{V vs. SCE}$
0.77	508	466	2.66	-1.89

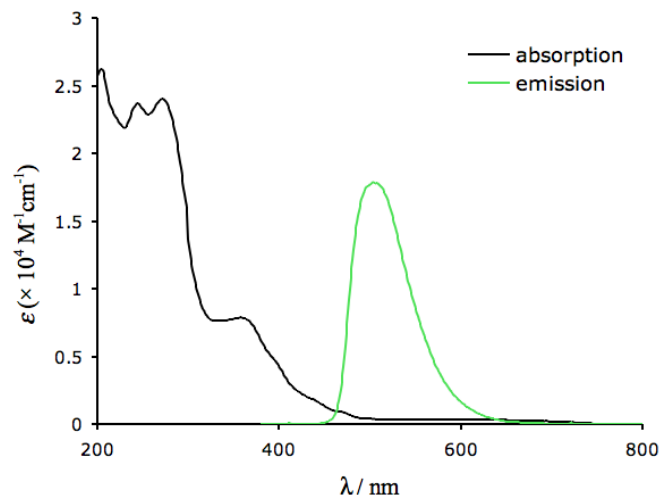


Fig. S2. UV-vis absorption and steady-state luminescence spectra of $\text{Na}_3[\text{Ir}(\text{sppy})_3]$ in water.

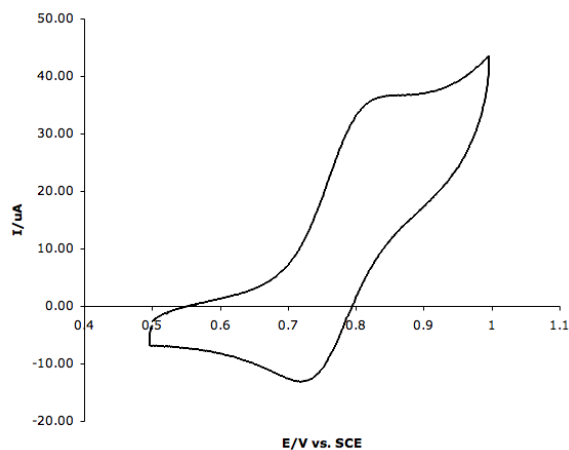


Fig. S3. Cyclic voltammogram for $\text{Na}_3[\text{Ir}(\text{sppy})_3]$ in 0.5 M aqueous phosphate buffer at pH 8.0.

3) Experimental details for the reactions with Na₃[Ir(sppy)₃] / *E. coli* (MAO-N-9)

General procedure (A) for the reduction of imines with Na₃[Ir(sppy)₃]

Imine or iminium ion substrate **1** (10 μmol) was dissolved in 1 mL of aqueous phosphate buffer solution (0.5 M, pH 8.0) containing ascorbic acid (36 mg, 0.2 mmol) and Na₃[Ir(sppy)₃] (0.1 μmol). The reaction mixture was irradiated with a 405 nm LED lamp (3W) for 10 hours at room temperature under air. The reaction was quenched with 0.5 mL of 2 M aqueous NaOH solution, then the mixture was extracted with 1 mL of CD₂Cl₂ or CDCl₃. After drying over anhydrous Na₂SO₄ the crude mixture was analyzed by ¹H NMR spectroscopy to determine the conversion of imine substrate **1** to amine product **2**.

General procedure (B) for the reduction of imines with Na₃[Ir(sppy)₃] and *E. coli* (MAO-N-9)

Imine or iminium ion substrate **1** (10 μmol) was dissolved in 1 mL of aqueous phosphate buffer solution (0.5 M, pH 8.0) containing ascorbic acid (36 mg, 0.2 mmol) and Na₃[Ir(sppy)₃] (0.1 μmol). *E. coli* (MAO-N-9) whole cells (180 mg) were added to the reaction solution to form an aqueous suspension. The reaction mixture was irradiated with a 405 nm LED lamp (3W) for 30 hours at room temperature under air on an agitator at 200 rpm. The reaction was quenched with 0.5 mL of 2 M aqueous NaOH solution, then the suspension was divided into several small portions which were subsequently extracted with 1 mL of CD₂Cl₂ or CDCl₃ to circumvent problems with phase separation that occurred when trying to extract everything at once. After drying with anhydrous Na₂SO₄ the crude mixture was analyzed by ¹H NMR spectroscopy to determine the conversion of imine substrate **1** to amine product **2**. In order to determine the enantiomeric excess for the reactions of **1a-d**, derivatizations of amine products **2a-d** to amides were carried out. Specifically, after ¹H NMR analysis the crude solution was treated with 0.2 mL of trifluoroacetic anhydride (TFAA) for 5 minutes, followed by removal of the solvent and excess TFAA by flushing nitrogen. The enantiomeric excess was determined by chiral GC, using an Agilent instrument of the 6890-series equipped with FID on a chiral stationary phase (CP-ChiraSil-DEX CB 25 m × 0.25 mm × 0.25 μm; 115 °C isothermal, 1.7 mL He/min; injector: 250 °C, split 30; detector: 240 °C). Assignment of absolute configuration is based on selectivities observed for MAO-N with analogous substrates.^{S7}

3.1 Identification of a suitable photocatalyst for 2-cyclohexyl-1-pyrroline (**1a**) reduction

Substrate **1a** (50 μmol) was dissolved in 1 mL of aqueous phosphate buffer solution (0.5 M, pH 8.0) containing ascorbic acid (18 mg, 0.1 mmol) and photocatalyst (0.5 μmol). The reaction mixture was irradiated with a 405 or 455 nm LED lamp (3W) at room temperature under air. Then, an aliquot of 0.1 mL was taken from the aqueous reaction mixture and added to 0.5 mL of D_2O to determine the conversion of **1a** to *rac*-**2a** by ^1H NMR analysis. For the reaction of **1a** with *fac*- $\text{Ir}(\text{ppy})_3$ photocatalyst, 1 mL of CD_3CN (with 10% H_2O) was used as the solvent.

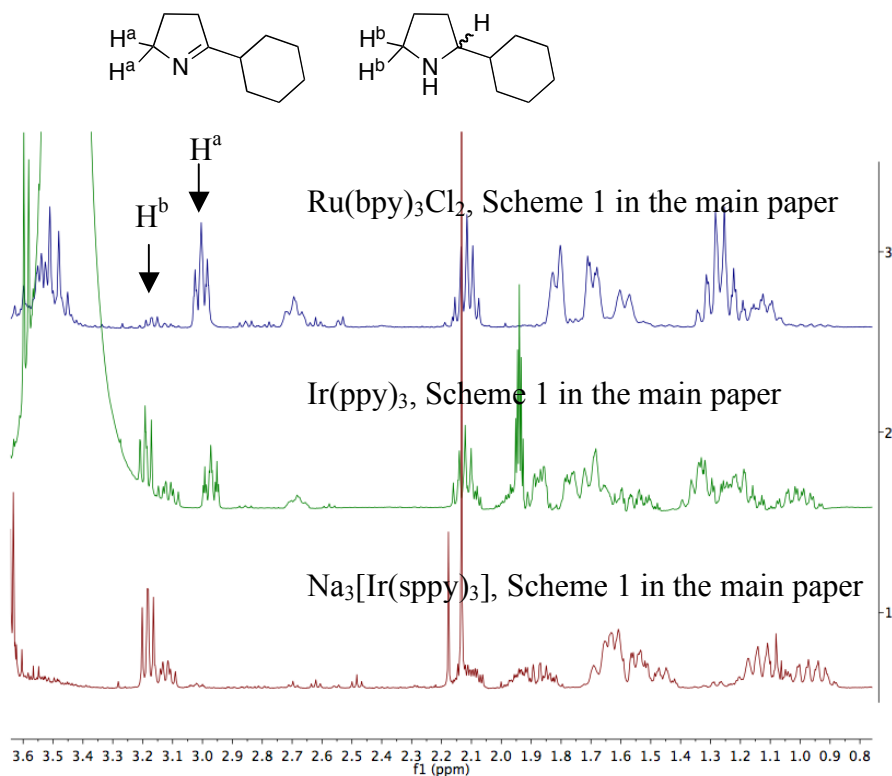


Fig. S4. ^1H NMR spectra of the crude reaction mixtures of 2-cyclohexyl-1-pyrroline (**1a**) reduction with different photocatalysts.

3.2 Reduction of 2-cyclohexyl-1-pyrroline (**1a**) with [Ir]/[MAO-N-9] system

General procedure B was followed for the reactions of **1a** in entries 1, 2, 4, 5 of Table 1 in the main paper. The *E. coli* cell lysate was obtained by ultrasonication of the reaction suspension containing *E. coli* (MAO-N-9) whole cells.

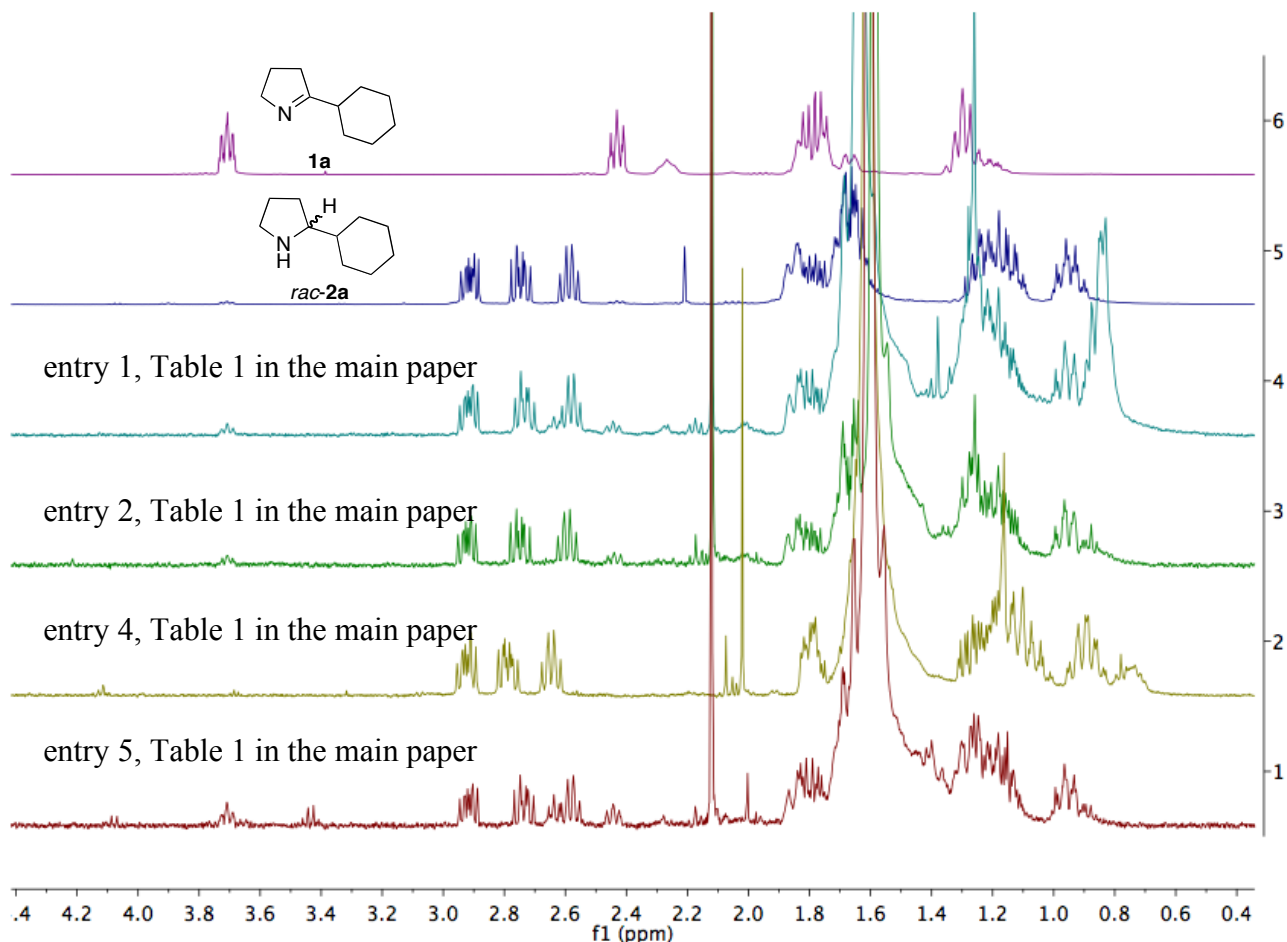


Fig. S5. ¹H NMR spectra of the crude reaction mixtures (organic extracts) of 2-cyclohexyl-1-pyrroline (**1a**) reduction with Na₃[Ir(sppy)₃] / *E. coli* (MAO-N-9). The two uppermost traces are the ¹H NMR spectra of the pure starting material (**1a**) and the product (*rac-2a*), respectively.

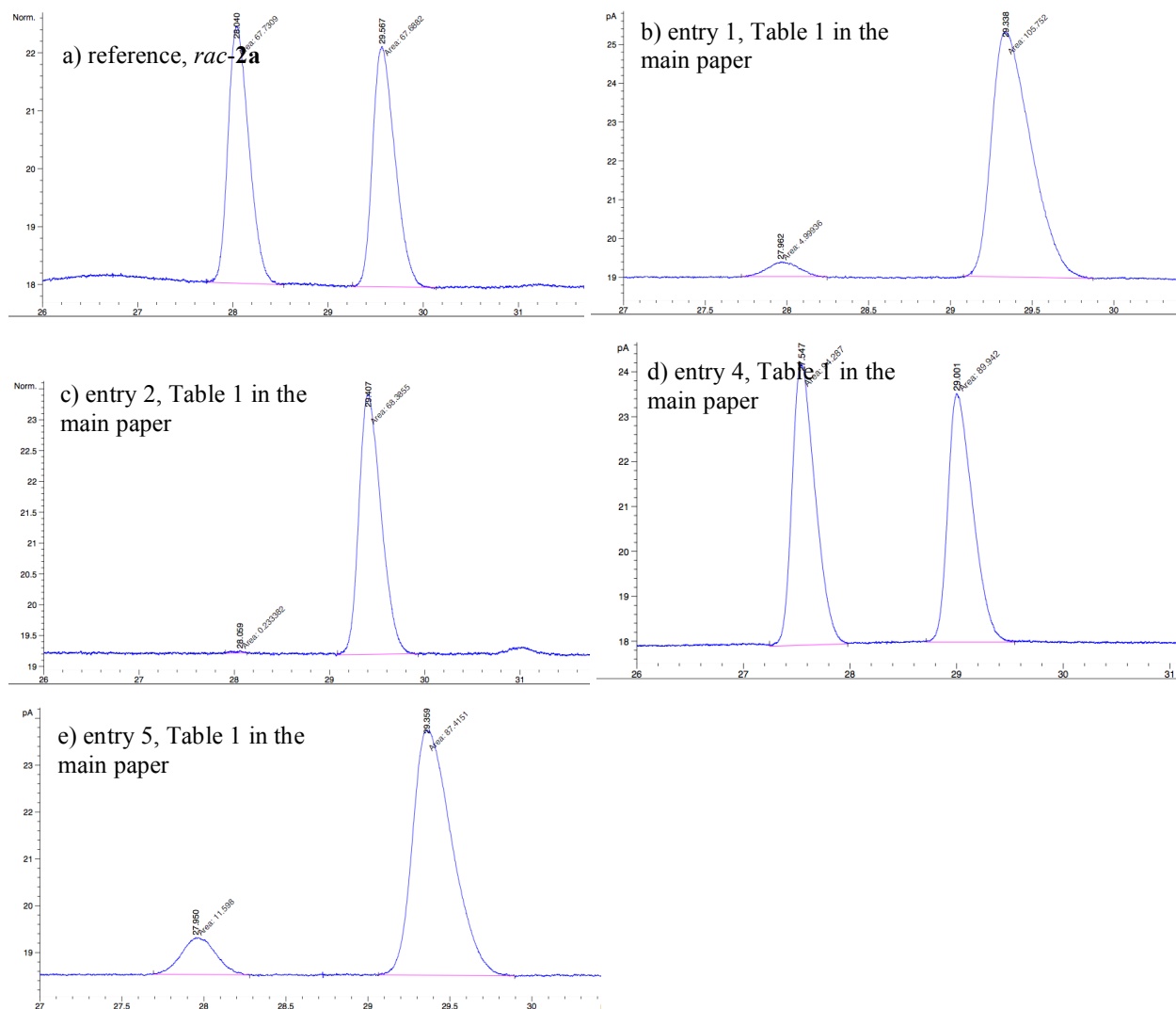
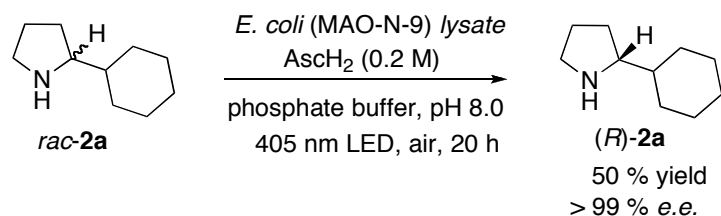


Fig. S6. Chiral phase GC traces showing the enantiomeric ratio between (*R*)-**2a** and (*S*)-**2a** resulting from the reduction of 2-cyclohexyl-1-pyrroline (**1a**) with $\text{Na}_3[\text{Ir}(\text{sppy})_3] / E. coli$ (MAO-N-9). The x-axes show retention times in minutes.

3.3 Kinetic resolution of 2-cyclohexyl-1-pyrrolidine *rac-2a* with *E. coli* (MAO-N-9) lysate

In order to examine whether photoredox and enzymatic catalysis mutually perturb each other in the cell lysate, we performed kinetic resolution experiments of *rac-2a* in *E. coli* (MAO-N-9) cell lysate (Scheme S2).



Scheme S2. Kinetic resolution of *rac-2a* using *E. coli* (MAO-N-9) lysate.

Under the same conditions listed in Table 1, entry 5 in the main paper but without photocatalyst, the kinetic resolution of *rac-2a* to afford *(R)-2a* is quantitative. This supports our hypothesis that the lowered enantioselectivity of the imine to amine reduction in the cell lysate (Table, 1 entry 5 in the main paper) is due to partial inactivation of MAO-N-9 by the photocatalyst. Conversely, the lower yield for the overall reaction (83%) is likely caused by a detrimental effect of the biocatalyst (or cellular debris) on the photoredox process.

General procedure B was followed for the deracemization reaction of *rac-2a* in Scheme 2 of the main paper, except that 2-cyclohexyl-1-pyrrolidine (*rac-2a*) was used as a substrate and *E. coli* cell lysate without photocatalyst was employed.

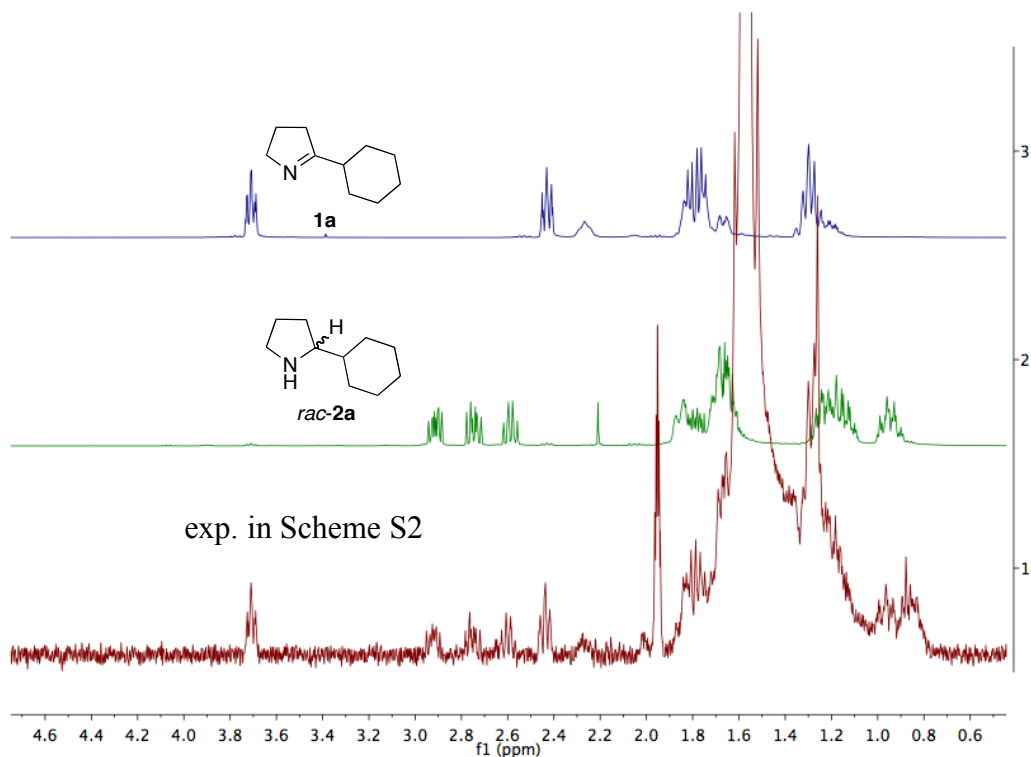


Fig. S7. Bottom trace: ^1H NMR spectrum of the crude reaction mixture (combined organic extracts) of 2-cyclohexyl-1-pyrrolidine (*rac-2a*) deracemization with *E. coli* (MAO-N-9) lysate. The top and the middle spectra are the ^1H NMR spectra of imine **1a** and amine *rac-2a*.

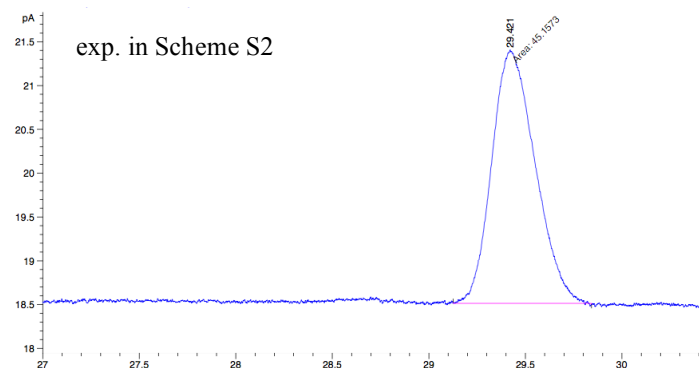


Fig. S8. Chiral phase GC trace of the 2-cyclohexyl-1-pyrrolidine (*rac-2a*) deracemization experiment with *E. coli* (MAO-N-9) lysate. Retention time in minutes is on the horizontal axis.

3.4 Reduction of 2-*n*-butyl-1-pyrroline (**1b**) with [Ir]/[MAO-N-9] system

General procedure A was followed for the reaction of **1b** in entry 1 of Table 2 in the main paper.

General procedure B was followed for the reaction of **1b** in entry 2 of Table 2 in the main paper.

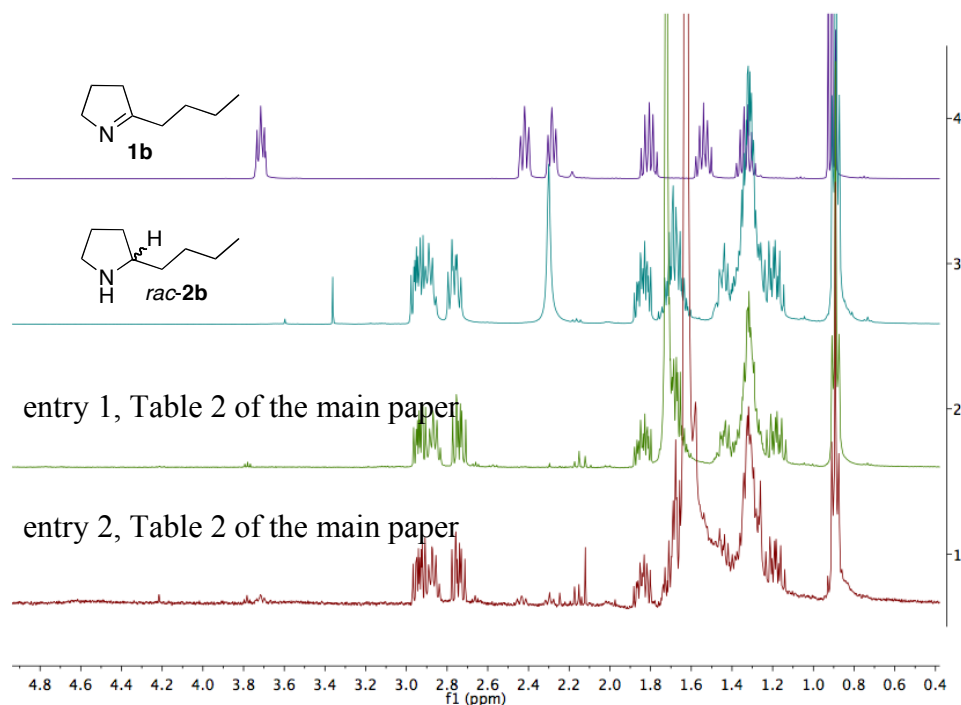


Fig. S9. ¹H NMR spectra of the crude reaction mixtures (organic extracts) resulting from 2-*n*-butyl-1-pyrroline (**1b**) reduction with Na₃[Ir(sppy)₃] / *E. coli* (MAO-N-9). The two uppermost traces are the ¹H NMR spectra of the pure starting material (**1b**) and product (*rac*-**2b**), respectively.

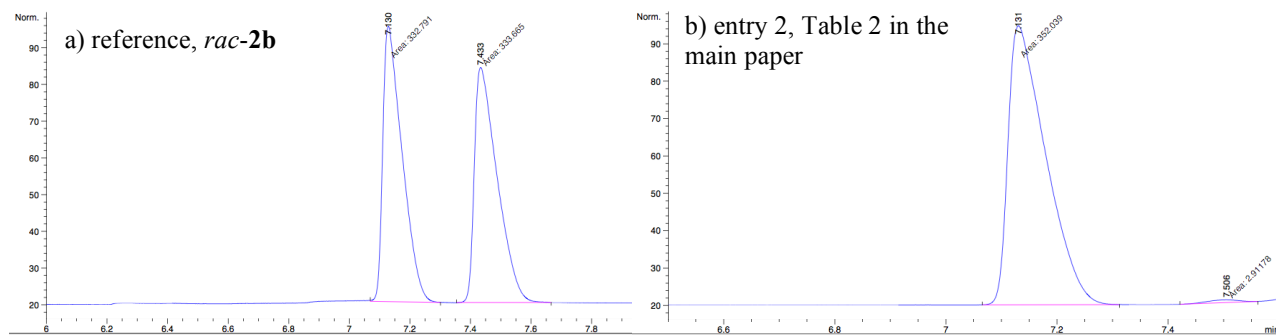


Fig. S10. Chiral phase GC traces showing the ratio between (*R*)-**2b** and (*S*)-**2b** as products of the reduction of 2-*n*-butyl-1-pyrroline (**1b**) with Na₃[Ir(sppy)₃] / *E. coli* (MAO-N-9). Retention times in minutes are on the horizontal axis.

3.5 Reduction of 2-benzyl-1-pyrroline (**1c**) with [Ir]/[MAO-N-9] system

General procedure A was followed for the reaction of **1c** in entry 3 of Table 2 in the main text.

General procedure B was followed for the reaction of **1c** in entry 4 of Table 2 in the main text.

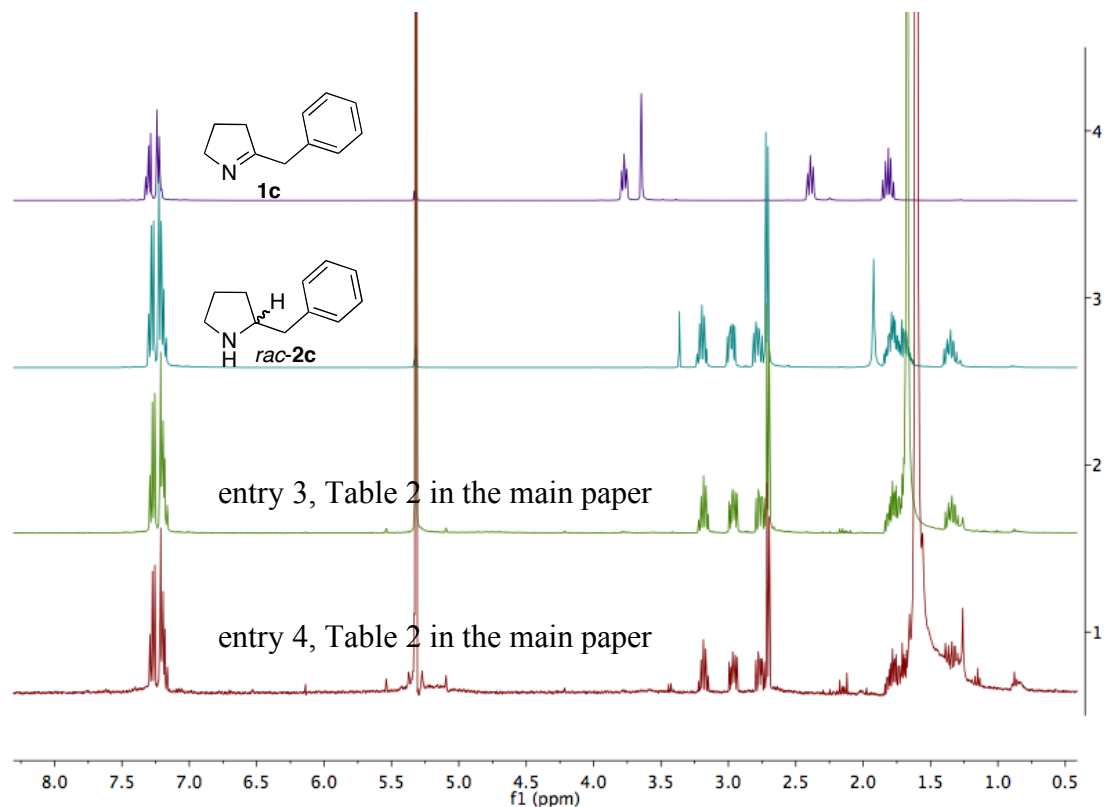


Fig. S11. ¹H NMR spectra of the crude reaction mixtures (organic extracts) of 2-benzyl-1-pyrroline (**1c**) reduction with Na₃[Ir(sppy)₃] / *E. coli* (MAO-N-9). The two uppermost traces are the ¹H NMR spectra of the pure starting material (**1c**) and product (*rac*-**2c**), respectively.

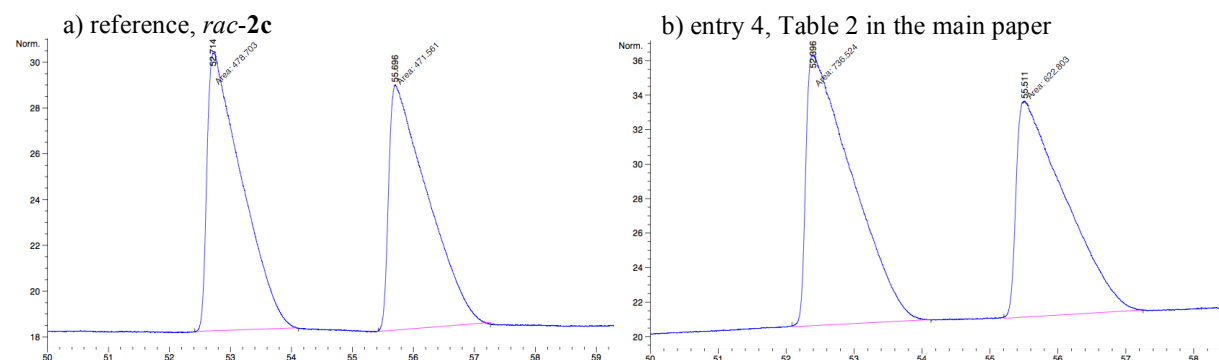


Fig. S12. Chiral phase GC traces showing the enantiomeric ratio between (*R*)-**2c** and (*S*)-**2c** resulting from 2-benzyl-1-pyrroline (**1c**) reduction with Na₃[Ir(sppy)₃] / *E. coli* (MAO-N-9). Retention times in minutes are on the horizontal axis.

3.6 Reduction of 2-cyclohexyl-1-methyl-pyrrolinium iodide (**1d**) with [Ir]/[MAO-N-9] system

General procedure A was followed for the reaction of **1d** in entry 5 of Table 2 in the main text.

General procedure B was followed for the reaction of **1d** in entry 6 of Table 2 in the main text.

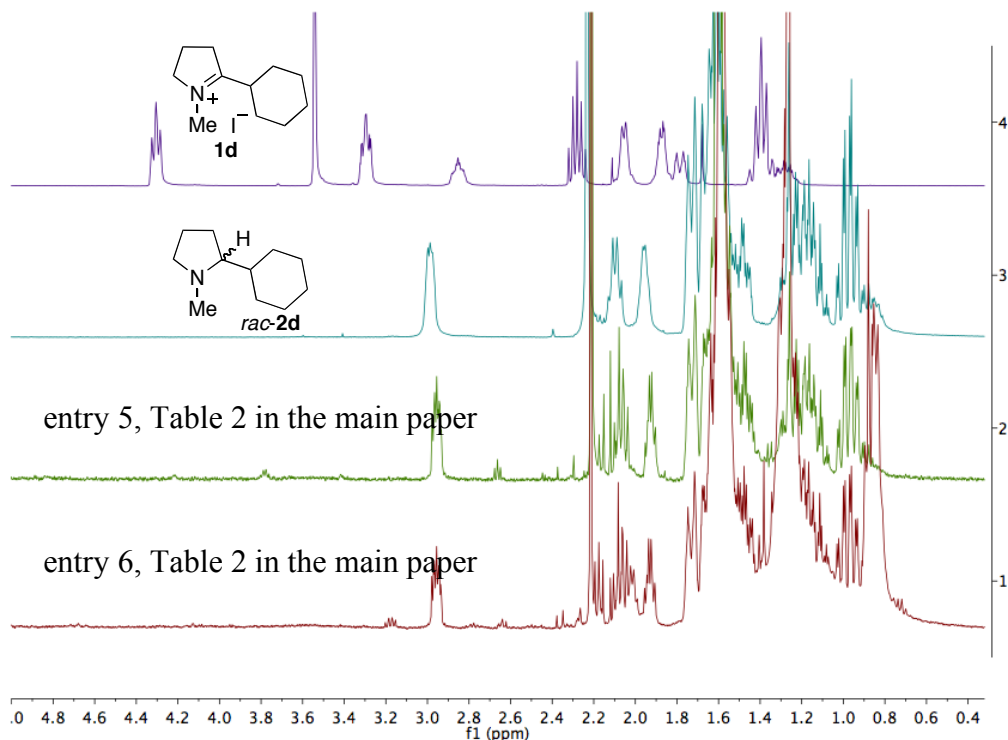


Fig. S13. ¹H NMR spectra of the crude reaction mixtures (organic extracts) of 2-cyclohexyl-1-methyl-pyrrolinium iodide (**1d**) reduction with Na₃[Ir(sppy)₃] / *E. coli* (MAO-N-9). The two uppermost traces are the ¹H NMR spectra of the pure starting material (**1d**) and product (*rac*-**2d**), respectively.

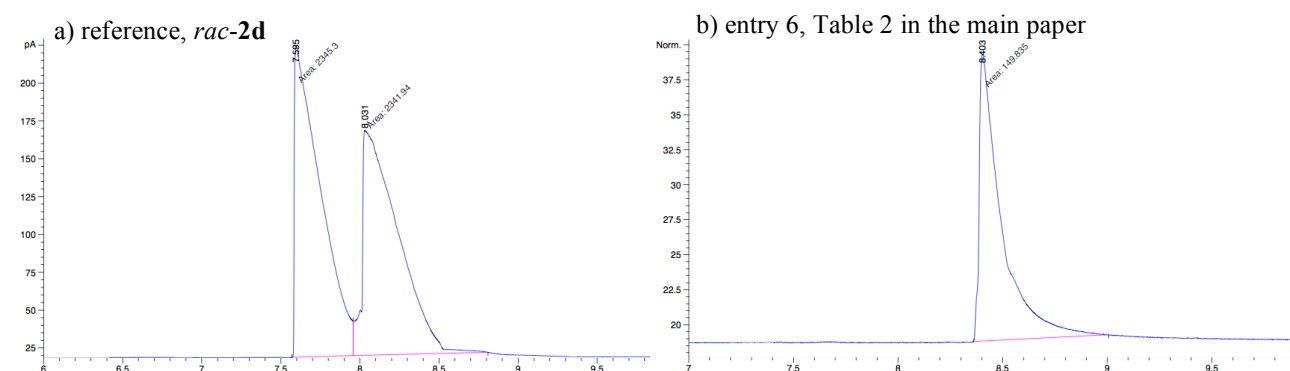


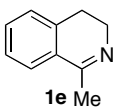
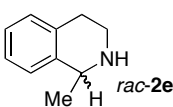
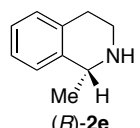
Fig. S14. Chiral phase GC traces showing the enantiomeric ratio between (*R*)-**2d** and (*S*)-**2d** resulting from reduction of 2-cyclohexyl-1-methyl-pyrrolinium iodide (**1d**) with Na₃[Ir(sppy)₃] / *E. coli* (MAO-N-9). Retention times in minutes are on the horizontal axis.

3.7 Reduction of 1-methyl-3,4-dihydroisoquinoline (**1e**) with [Ir or Ru]/[MAO-N-9] system

Using the standard photoredox conditions for aromatic substrate **1e**, no amine **2e** was formed (Table S2, entry 1), even though there is sufficient driving-force for the initial photoinduced electron transfer from $\text{Na}_3[\text{Ir}(\text{sppy})_3]$ to the substrate. (The emissive excited state is quenched rapidly, see Table S6). Consequently, we hypothesized that the ensuing HAT process between ascorbic acid and the photochemically-generated α -amino alkyl radical intermediates is too slow. This in turn is likely due to significant stabilization of the respective carbon-centered radical in the aromatic substrate, rendering the HAT process considerably less exergonic than in the case of aliphatic substrates. Therefore, we attempted to lower the activation barrier for HAT by adding 3-mercaptopropionic acid (MPA) (Fig. S15a), hypothesizing that polarity-matched HAT between this thiol donor and the α -amino alkyl radical intermediates would proceed sufficiently rapidly.^{S8} Thiyl radicals formed in the course of this reaction could then be regenerated to thiols by subsequent HAT from ascorbic acid (Fig. S15b).^{S8a} On the other hand, the lack of conversion in entry 1 (Table S2) might be also caused by fast back electron transfer (BET) following oxidative quenching of the excited state of $\text{Na}_3[\text{Ir}(\text{sppy})_3]$ by substrate **1e**, which results in a non-productive quenching process. We anticipated that by using $[\text{Ru}(\text{bpy})_3]\text{Cl}_2$ instead of $\text{Na}_3[\text{Ir}(\text{sppy})_3]$ the non-productive oxidative quenching and BET processes could be suppressed, because ³MLCT-excited $[\text{Ru}(\text{bpy})_3]\text{Cl}_2$ can be quenched very rapidly by ascorbate.^{S9} The resulting $[\text{Ru}(\text{bpy})_3]^+$ species is able to reduce **1e** to the α -amino alkyl radical intermediate without competition from back electron transfer. When using both AscH_2 (50 mM) and MPA (0.2 M) as reducing agents, and $[\text{Ru}(\text{bpy})_3]\text{Cl}_2$ as a photosensitizer, 17% of the desired product *rac*-**2e** was obtained after 10 hours (Table S2, entry 2). While this validates the usefulness of a thiol additive, the modest yield suggests that HAT is still too slow, and therefore we added an aromatic thiol, 4-mercaptophenylacetic acid (MPAA), which has a lower S–H bond dissociation energy (BDE) than MPA (Fig. S15a).^{S10} To our delight, *rac*-**2e** was obtained in quantitative yield (>95%) when using a combination of AscH_2 , MPAA, MPA and $[\text{Ru}(\text{bpy})_3]\text{Cl}_2$ as photocatalyst (Table S2, entry 3), suggesting that the aromatic carbon-centered radical intermediate is readily intercepted by HAT from MPAA (HAT_a in Fig. S15b). The aromatic thiyl species formed in this process subsequently reacts with ascorbate (HAT_b in Fig. S15b) via polarity-matched HAT.^{S8} Given the observed accumulation of aliphatic disulfide as a final oxidation product, the main function of MPA seems to be the regeneration of dehydroascorbic acid to ascorbate (polar reaction in Fig. S15b). The necessity for the presence of both aromatic (MPAA) and aliphatic thiols (MPA) is likely due to the fact that aromatic disulfides can

be re-activated to thiyls upon irradiation of the photocatalyst, whilst the aliphatic disulfide is a stable oxidation product under these conditions (for reference, the one-electron reduction potential of diphenyl disulfide is -1.37 V vs. SCE while that for dimethyl disulfide is -1.88 V vs. SCE).^{S11}

Table S2. Reaction condition optimization for **1e**.

entry	substrate	photocat. & reducing agent	biocat.	product	yield [e.e.] (%)
1		Na ₃ Ir(sppy) ₃ (1 mol %) + AsCH ₂ (0.2 M)	—		0
2	1e	Ru(bpy) ₃ Cl ₂ (1 mol %) + AsCH ₂ (50 mM) + MPA (0.2 M)	—	<i>rac</i> - 2e	17
3	1e	Ru(bpy) ₃ Cl ₂ (1 mol %) + AsCH ₂ (50 mM) + MPAA (0.2 M) + MPA (0.2 M)	—	<i>rac</i> - 2e	> 95
4	1e	Ru(bpy) ₃ Cl ₂ (1 mol %) + AsCH ₂ (50 mM) + MPAA (0.2 M) + MPA (0.2 M)	MAO-N-9 (180 mg)		> 95[0]

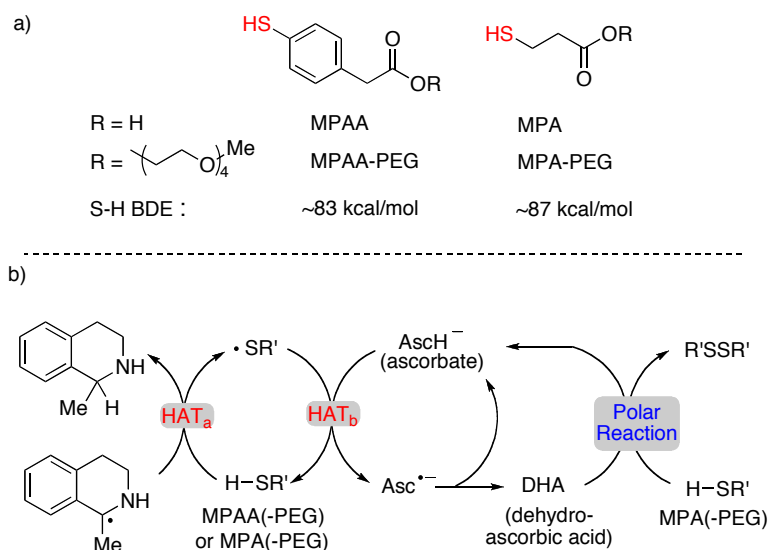


Fig. S15. The presumed mechanism of polarity-matched HAT with thiols.

The photodriven conversion of **1e** to **2e** proceeded to completion in combination with *E. coli* whole cells containing the MAO-N-9 biocatalyst. Unfortunately, no enantioselectivity was observed in initial

experiments (Table S2, entry 4). We hypothesize that the breakdown of the cyclic reaction network in this case might be due to deactivation of MAO-N-9 by the high concentration of thiols^{S12} or because MPAA potentially acts as an inhibitor of MAO-N-9. To overcome this challenge, we modified the thiols by esterification with tetraethyleneglycol monomethyl ether (short PEG chain), anticipating that this could impede diffusion of the modified thiols into the enzyme and minimize undesired interactions with the active site. This strategy was indeed successful as noted in the main paper.

General procedure A was followed for the reaction of **1e** in entry 7 of Table 2 in the main text.

General procedure A was followed for the reaction of **1e** in entry 8 of Table 2 in the main text, except that [Ru(bpy)₃]Cl₂ (1 mol%) was used as a photocatalyst, and MPA (0.2M) with AscH₂ (50 mM) were used as reducing agents / H-atom donors.

General procedure A was followed for the reaction of **1e** in entry 9 of Table 2 in the main text, except that [Ru(bpy)₃]Cl₂ (1 mol%) was used as a photocatalyst, and MPA (0.2 M), MPAA (0.2 M) and AscH₂ (50 mM) were used as reducing agents / H-atom donors, and the reaction time was 3 h.

General procedure B was followed for the reaction of **1e** in entry 10 of Table 2 in the main text, except that [Ru(bpy)₃]Cl₂ (1 mol%) was used as a photocatalyst, and MPA (0.2 M), MPAA (0.2 M) and AscH₂ (50 mM) were used as reducing agents / H-atom donors, and the reaction time was 20 h. In this case, the enantiomeric excess was determined by chiral HPLC without derivatization of the amine product. HPLC measurements were performed on a Shimadzu Prominence system with SIL-20A auto sample, CTO-20AC column oven, LC-20AD pump system, DGU-20A3 degasser and SPD-M20A diode array or UV/VIS detector (chiral column: Daicel IC 250 × 4.6 mm × 5 μm; hexane/*i*-PrOH/HNEt₂ = 97/3/0.03, 1 mL/min, 25 °C, 265 or 234 nm).

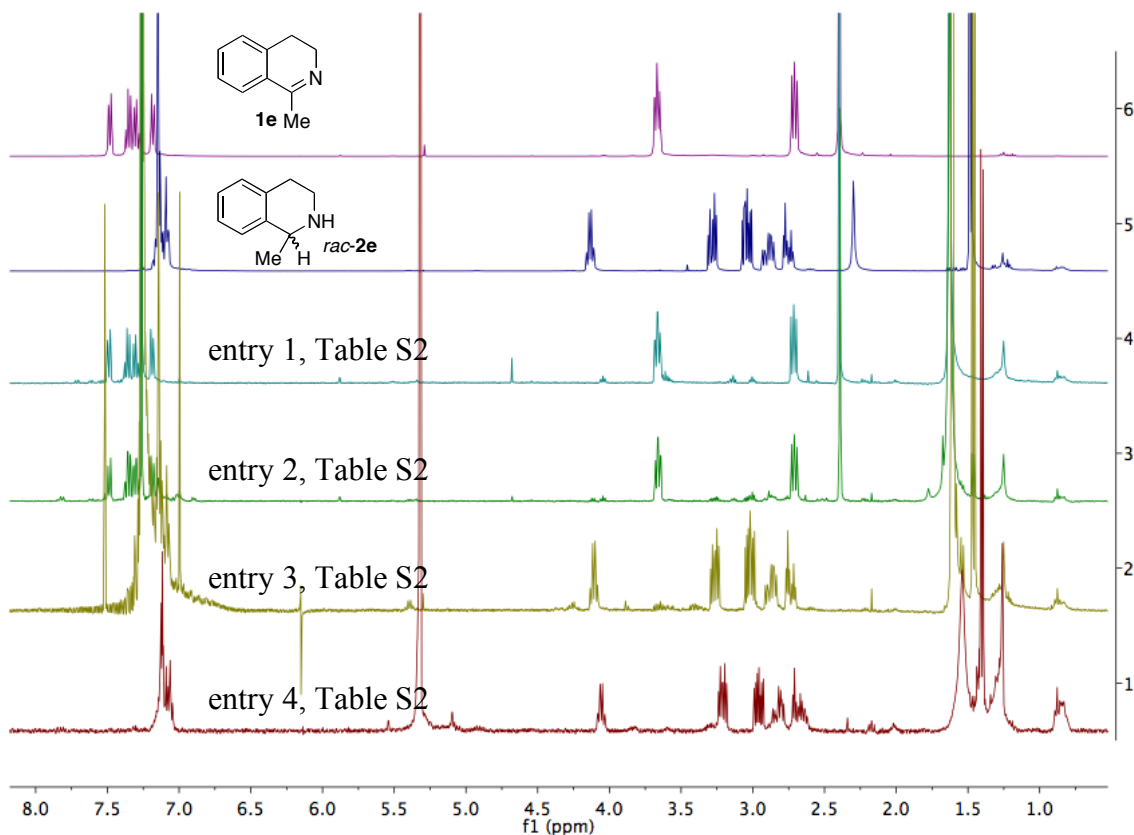


Fig. S16. Lower four traces: ^1H NMR spectra of the crude reaction mixtures (organic extracts) obtained after reaction of 1-methyl-3,4-dihydroisoquinoline (**1e**) under various conditions. The two uppermost traces are the ^1H NMR spectra of the pure starting material (**1e**) and product (*rac*-**2e**), respectively.

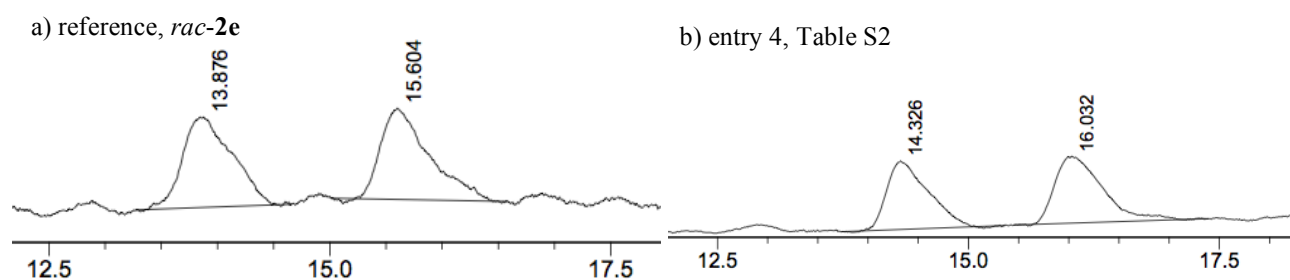
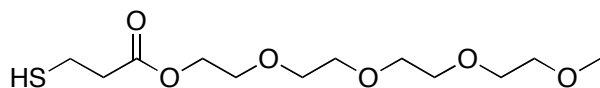


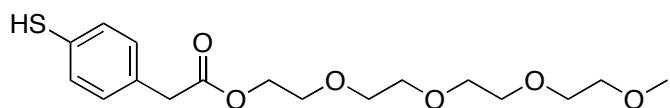
Fig. S17. Chiral phase HPLC traces showing the enantiomeric ratio between (*R*)-**2e** and (*S*)-**2e** resulting from reduction of 1-methyl-3,4-dihydroisoquinoline (**1e**) using MPA/MPAA/Asch₂ with photocatalyst/biocatalyst. Retention times in minutes are on the horizontal axis.

Procedure for the modification of MPA (and MPAA):

3-mercaptopropionic acid (MPA) (11 mmol) and tetraethyleneglycol monomethyl ether (10 mmol) were dissolved in 20 mL of toluene in a 50 mL flask equipped with a Dean-Stark water separator and a cooling condenser. After adding *p*-toluenesulfonic acid (1 mmol%) into the solution, the reaction mixture was heated to reflux. After 12 h the reaction mixture was allowed to cool down to room temperature and was washed with 5 mL saturated aqueous NaHCO₃ solution. The organic layer was collected and the solvent removed under reduced pressure. The residue was purified rapidly on a short column of silica gel using acetone/dichloromethane (1:1) as the eluent and working under inert atmosphere to avoid aerobic oxidation. After removing the solvent, the desired product was obtained as a colorless oil in 85% yield. The product should be stored under inert atmosphere.



2,5,8,11-tetraoxatridecan-13-yl 3-mercaptopropanoate (MPA-PEG). IR (neat): ν_{\max} 2874, 2560, 1733, 1453, 1349, 1248, 1197, 1102, 944, 853 cm⁻¹; ¹H NMR (CDCl₃, 400 MHz) δ 4.27-4.24 (m, 2H), 3.71-3.68 (m, 2H), 3.66-3.62 (m, 10H), 3.37 (s, 3H), 2.79-2.73 (m, 2H), 2.70-2.65 (m, 2H), 1.67 (t, *J* = 8.3 Hz, 1H); ¹³C NMR (CDCl₃, 101 MHz) δ 171.7, 72.1, 70.7, 70.7, 70.7, 70.6, 69.2, 63.9, 59.2, 38.5, 19.9; HRMS (*m/z*) calcd for C₁₂H₂₄NaO₆S [M+Na⁺]: 319.1186; found: 319.1189.



2,5,8,11-tetraoxatridecan-13-yl 2-(4-mercaptophenyl)acetate (MPAA-PEG). The same procedure as described above for MPA was also used for the modification of 4-mercaptophenyl acetic acid (MPAA). MPAA-PEG was obtained as a colorless oil in 90% yield. IR (neat): ν_{\max} 2874, 2541, 1733, 1453, 1333, 1248, 1099, 1038, 946, 849, 804 cm⁻¹; ¹H NMR (CDCl₃, 400 MHz) δ 7.22 (d, *J* = 8.3 Hz, 2H), 7.15 (d, *J* = 8.3 Hz, 2H), 7.24-7.22 (m, 2H), 3.68-3.53 (m, 16H), 3.43 (s, 1H), 3.37 (s, 3H); ¹³C NMR (CDCl₃, 101 MHz) δ 171.5, 131.6, 130.2, 129.7, 129.6, 72.0, 70.7, 70.7, 70.7, 70.6, 69.1, 64.2, 59.2, 40.7; HRMS (*m/z*) calcd for C₁₇H₂₆NaO₆S [M+Na⁺]: 381.1342; found: 381.1347.

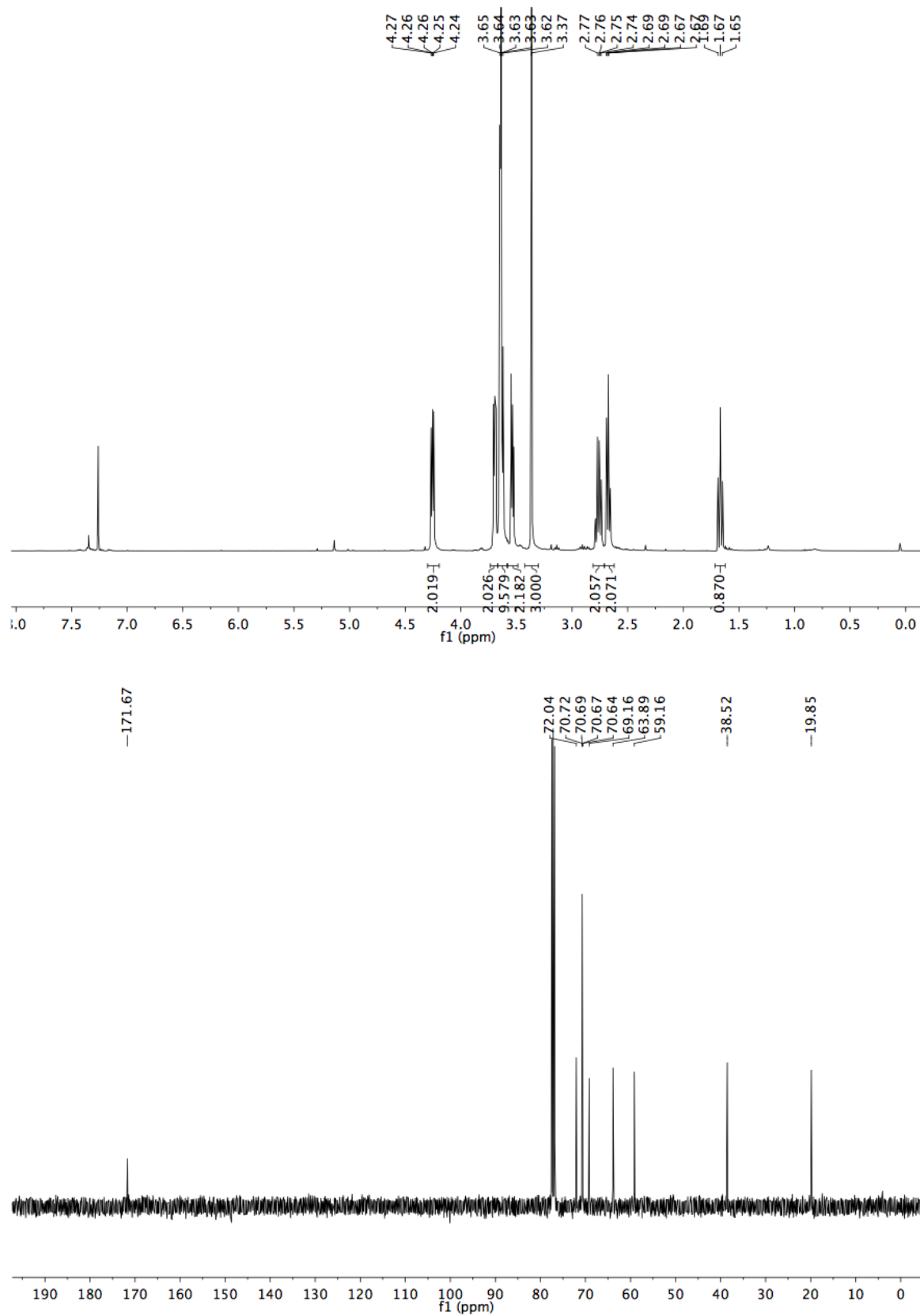


Fig. S18. ¹H and ¹³C NMR spectra of MPA-PEG in CDCl₃.

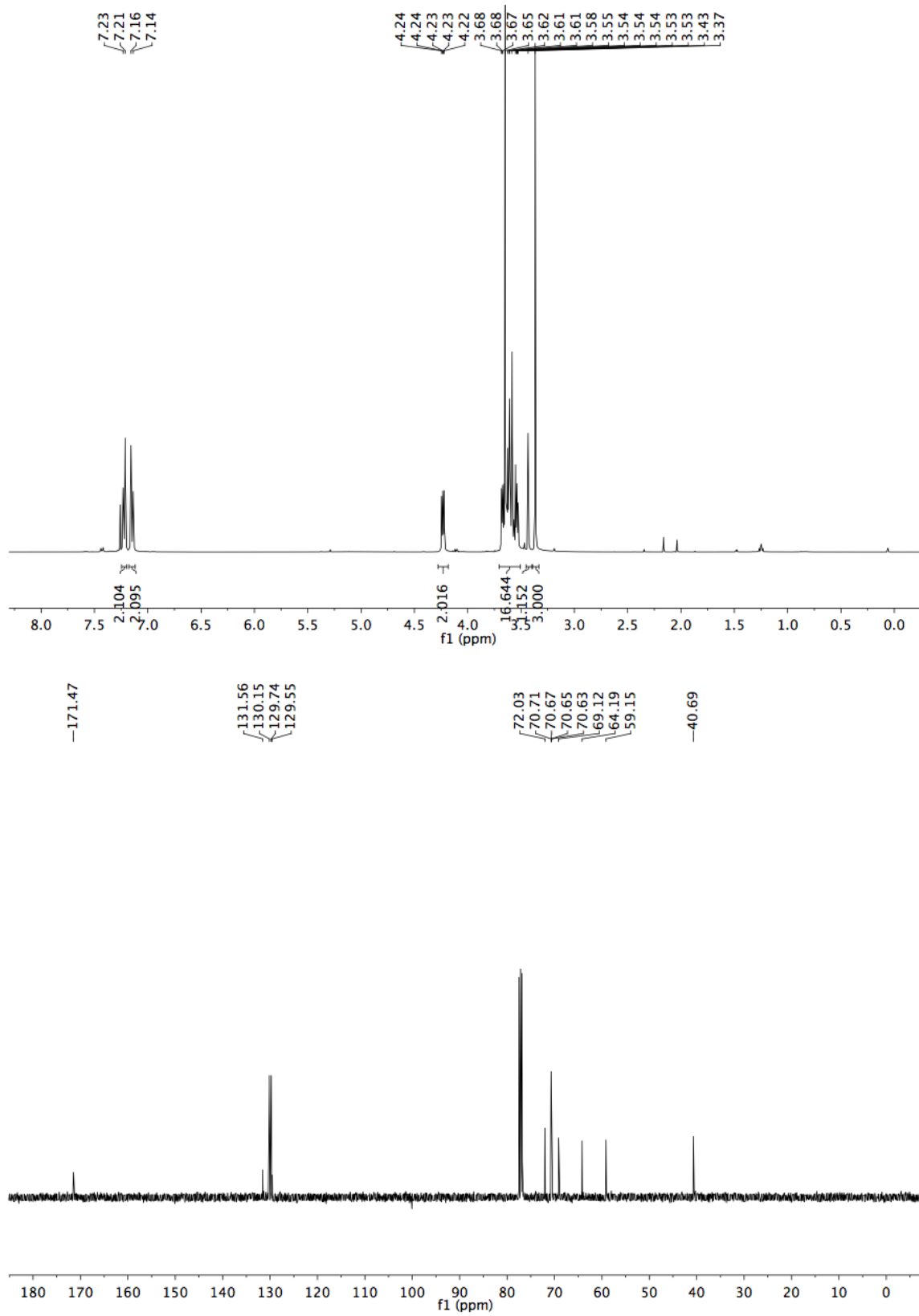


Fig. S19. ¹H and ¹³C NMR spectra of MPAA-PEG in CDCl₃.

Procedure for the reaction of 1e in entry 7 of Table 2 in the main text.

Imine substrate **1e** (10 μmol) was dissolved in 1 mL of aqueous phosphate buffer solution (0.5 M, pH 8.0) containing ascorbic acid (36 mg, 0.05 mmol), MPA-PEG (1 mmol), MPAA-PEG (0.1 mmol) and $[\text{Ru}(\text{bpy})_3]\text{Cl}_2$ (0.1 μmol). The reaction mixture was irradiated with a 450 nm LED lamp (3W) for 3 hours at room temperature under air on an agitator at 250 rpm. The reaction was quenched with 0.2 mL of 37% aqueous HCl solution. The mixture was extracted with 3×1 mL of CDCl_3 , the organic phase was discarded, the aqueous phase was treated with 0.5 mL of 40% aqueous NaOH solution, then the mixture was extracted with 1 mL of CDCl_3 . After drying over anhydrous Na_2SO_4 the crude mixture was analyzed by ^1H NMR spectroscopy to determine the conversion of imine substrate **1e** to amine product **2e**.

Note: MPA-PEG and MPAA-PEG are not fully soluble in aqueous solution, and therefore the reaction was performed under biphasic conditions.

Procedure for the reaction of 1e in entry 8 of Table 2 in the main text.

Imine substrate **1e** (10 μmol) was dissolved in 1 mL of aqueous phosphate buffer solution (0.5 M, pH 8.0) containing ascorbic acid (36 mg, 0.05 mmol), MPA-PEG (1 mmol), MPAA-PEG (0.1 mmol) and $[\text{Ru}(\text{bpy})_3]\text{Cl}_2$ (0.1 μmol). *E. coli* (MAO-N-9) whole cells (180 mg) were added to the reaction mixture to form an aqueous suspension. This mixture was irradiated with a 450 nm LED lamp (3W) for 20 hours at room temperature under air on an agitator at 250 rpm. The reaction was quenched with 0.2 mL of 37% aqueous HCl solution. The mixture was extracted with 3×3 mL of CDCl_3 , the organic phase was discarded, the aqueous phase was treated with 0.5 mL of 40% aqueous NaOH solution, then the suspension was divided into several small portions which were subsequently extracted with 1 mL of CDCl_3 to circumvent problems with phase separation that occurred when trying to extract everything at once. After drying over anhydrous Na_2SO_4 the crude mixture was analyzed by ^1H NMR spectroscopy to determine the conversion of imine substrate **1e** to amine product **2e**. The enantiomeric excess was determined by chiral HPLC as described above.

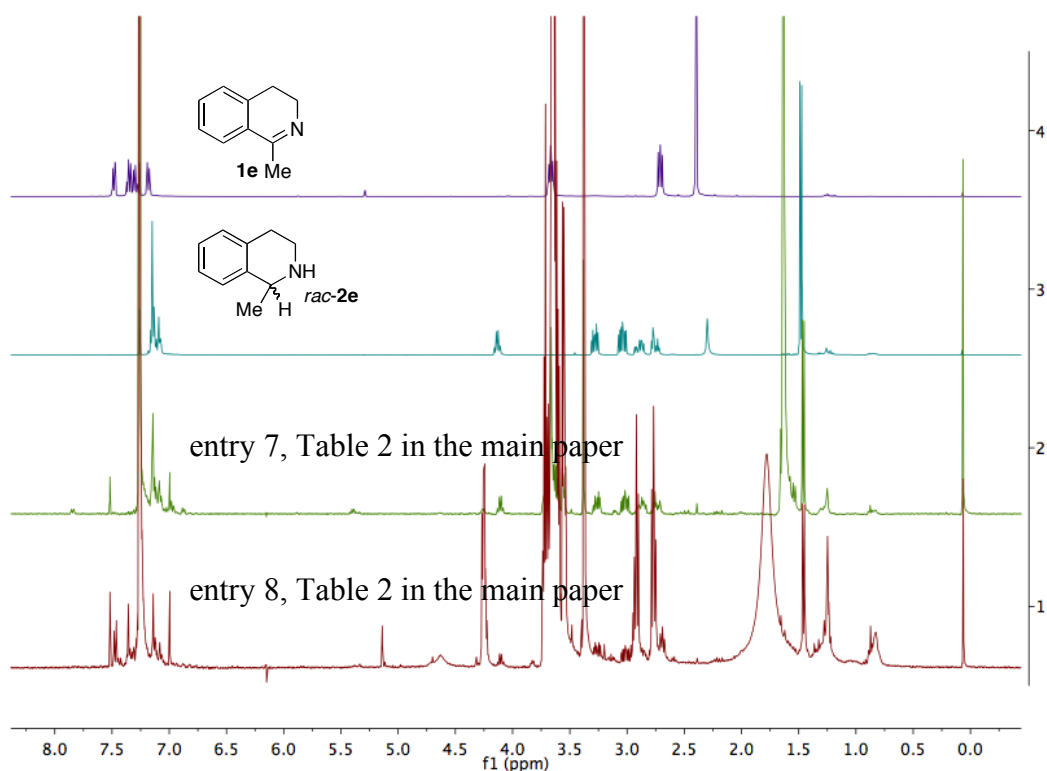
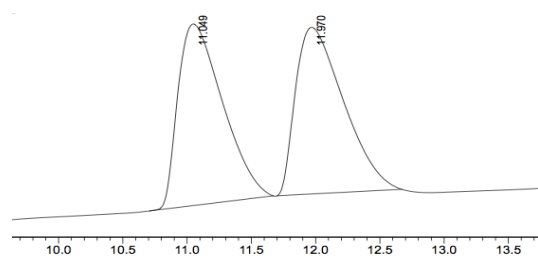


Fig. S20. Lower two traces: ^1H NMR spectra of the crude reaction mixtures (organic extracts) obtained after reaction of 1-methyl-3,4-dihydroisoquinoline (**1e**) using MPA-PEG/MPAA-PEG/Asch₂. The two uppermost traces are the ^1H NMR spectra of the pure starting material (**1e**) and product (*rac*-**2e**), respectively. The solvent was CDCl₃.

a) reference, *rac*-**2e**



b) entry 8, Table 2 in the main paper

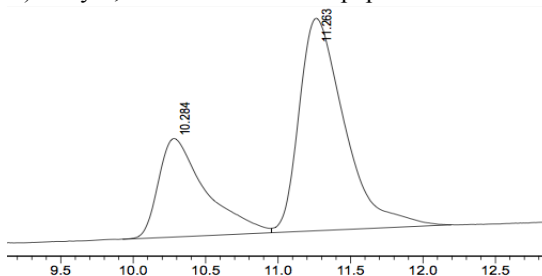


Fig. S21. Chiral phase HPLC traces showing the enantiomeric ratio between (*R*)-**2e** and (*S*)-**2e** resulting from reduction of 1-methyl-3,4-dihydroisoquinoline (**1e**) using MPA-PEG/MPAA-PEG/Asch₂ with photocatalyst/biocatalyst. Retention times in minutes are on the horizontal axis.

Somewhat different retention times were observed for the reference compound *rac*-**2e** between Fig. S17 and S21. The reason for this observation is not known, however, racemic reference compound was

always measured to compare with the reaction sample, and only minor differences in retention times (< 1 min) were observed in each case.

4) Monitoring the conversion of **1a** to (*R*)-**2a** by chiral GC as a function of time

The reactions were carried out according to general procedure B with 2 mol % Na₃[Ir(sppy)₃]. After each time point indicated in Fig. 2 of the main paper, a small portion of the reaction mixture (50 μL) was removed and worked up with 0.2 mL of 2 M aqueous NaOH solution, followed by extraction with 1 mL of CH₂Cl₂. After drying over anhydrous Na₂SO₄, the crude mixture was treated with 0.2 mL of trifluoroacetic anhydride (TFAA), and after removing the solvent and excess TFAA by flushing nitrogen, the conversion and enantiomeric excess were determined by chiral GC. As the data listed in Table S3 were directly calculated from the relative peak integrals of the components by the GC measurements without calibration curve, a comparatively low accuracy of the conversion data is expected for the data in Fig. 2 of the main paper. We estimate that experimental uncertainties in conversions in Table S3 are approximately ± 3 %.

Table S3. The time course of the reaction of **1a** to (*R*)-**2a** as monitored by chiral GC.

reaction time /h	1a /%	(<i>R</i>)- 2a /%	(<i>S</i>)- 2a /%	conv. /%	<i>e.e.</i> /%
0	100	0	0	0	0
1	15	46	39	85	8
2	7	56	37	93	20
3	7	63	30	93	35
4	8	72	20	92	57
6	13	78	9	87	79
8	10	87	3	90	93
10	13	86	1	87	98

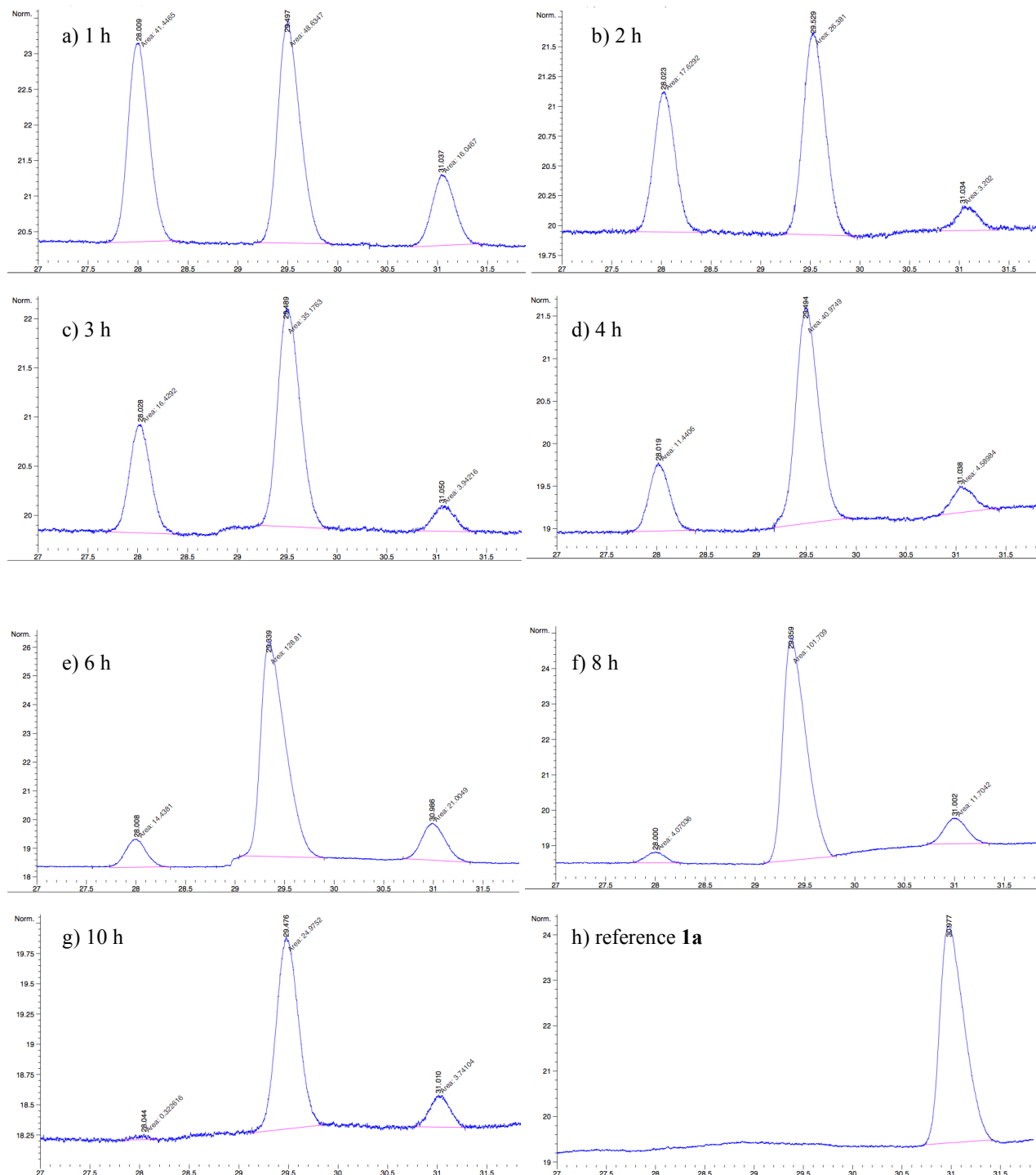


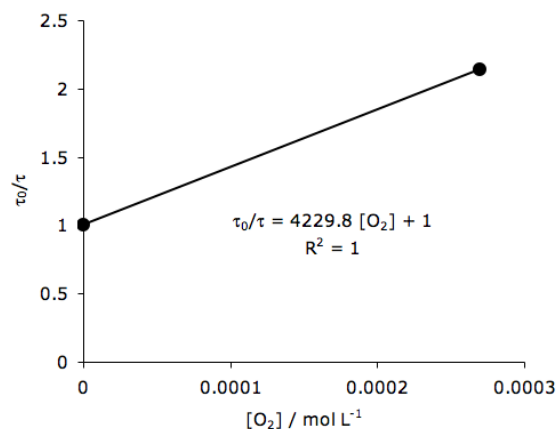
Fig. S22. Monitoring the conversion of **1a** to (*R*)-**2a** by chiral GC. Retention times in minutes are on the horizontal axes.

5) Luminescence quenching experiments with Na₃[Ir(sppy)₃]

Table S4. Luminescence quenching of Na₃[Ir(sppy)₃] by oxygen (under air) in water at pH 8.0 (1 atm, 20 °C, excitation at 405 nm, emission at 510 nm). A two-point Stern-Volmer plot is shown on the right.

[Na ₃ Ir(sppy) ₃] / mol L ⁻¹	[O ₂] / mol L ⁻¹	τ / μs
2.0 × 10 ⁻⁵	— (Ar)	1.493
2.0 × 10 ⁻⁵	2.7 × 10 ⁻⁴ ^a	0.697

$$k_q = 2.8 \times 10^9 \text{ L mol}^{-1} \text{ s}^{-1}$$



[a] according to the solubility of oxygen in water at 1 atm and 20 °C from ref S13.

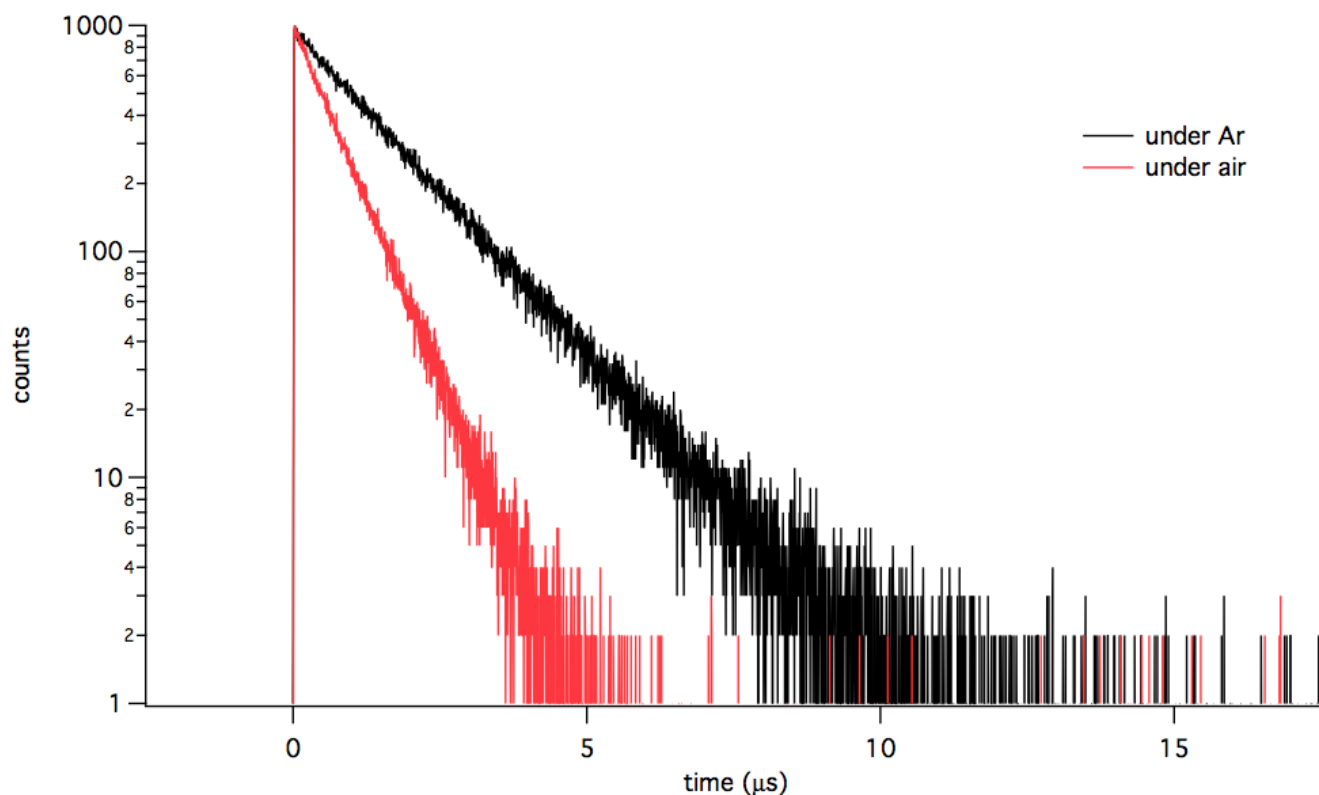


Fig. S23. Luminescence decays of a 20 μM solution of Na₃[Ir(sppy)₃] in aqueous phosphate buffer at pH 8. Excitation occurred at 405 nm, detection was at 510 nm.

Table S5. Luminescence quenching of $\text{Na}_3[\text{Ir}(\text{sppy})_3]$ by sodium ascorbate in water at pH 8.0 (20 °C, excitation at 405 nm, emission at 510 nm). A Stern-Volmer plot is shown on the right.

$[\text{Na}_3\text{Ir}(\text{sppy})_3]$ / mol L ⁻¹	$[\text{NaAscH}]$ / mol L ⁻¹	τ / μs
2.0×10^{-5}	—	1.493
2.0×10^{-5}	1.0×10^{-2}	1.392
2.0×10^{-5}	2.0×10^{-2}	1.288
2.0×10^{-5}	3.0×10^{-2}	1.206
2.0×10^{-5}	4.0×10^{-2}	1.144
2.0×10^{-5}	5.0×10^{-2}	1.081

$k_q = 5.1 \times 10^6 \text{ L mol}^{-1} \text{ s}^{-1}$

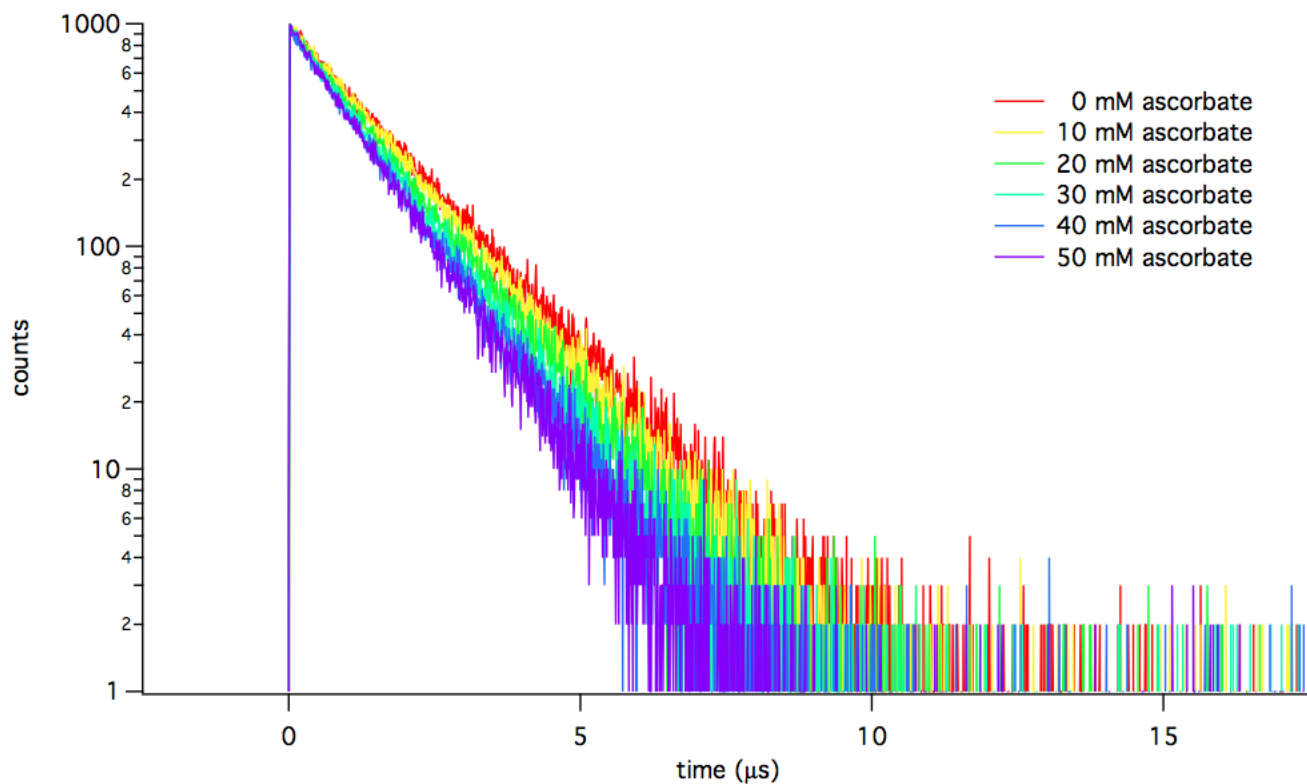
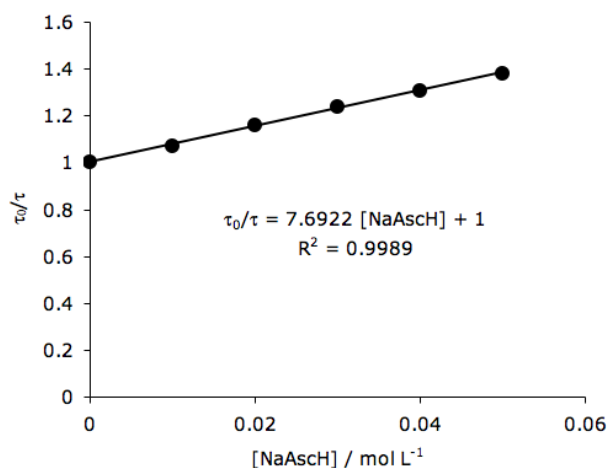


Fig. S24. Luminescence decays of $\text{Na}_3[\text{Ir}(\text{sppy})_3]$ in presence of ascorbate in aqueous phosphate buffer at pH 8.

Table S6. Luminescence quenching of $\text{Na}_3[\text{Ir}(\text{sppy})_3]$ by imine **1a** in water at pH 8.0 (20 °C, excitation at 405 nm, emission detected at 510 nm). A Stern-Volmer plot is shown on the right.

$[\text{Na}_3\text{Ir}(\text{sppy})_3]$ / mol L ⁻¹	$[\mathbf{1a}]$ / mol L ⁻¹	τ / μs
2.0×10^{-5}	—	1.493
2.0×10^{-5}	1.0×10^{-2}	1.414
2.0×10^{-5}	2.0×10^{-2}	1.339
2.0×10^{-5}	3.0×10^{-2}	1.299
2.0×10^{-5}	4.0×10^{-2}	1.262
2.0×10^{-5}	5.0×10^{-2}	1.231

$k_q = 2.8 \times 10^6 \text{ L mol}^{-1} \text{ s}^{-1}$

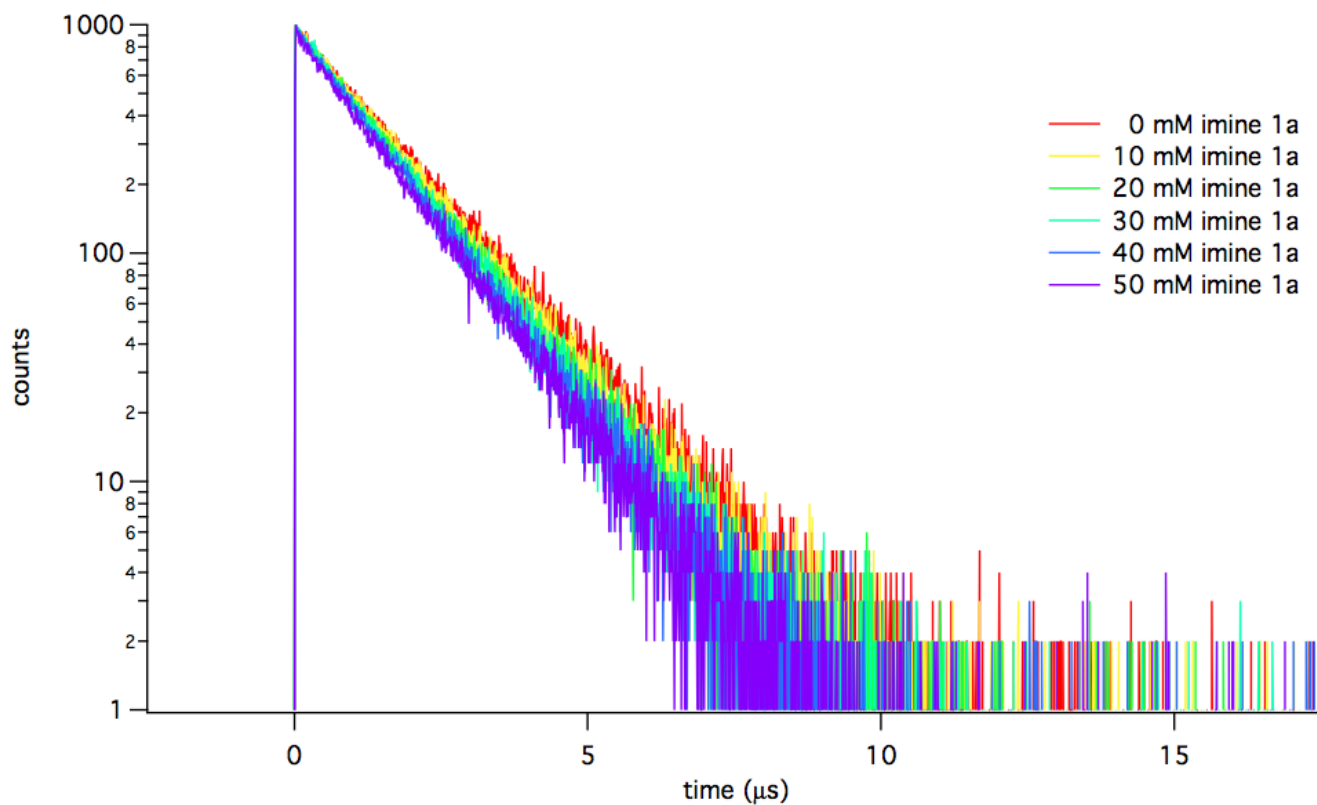
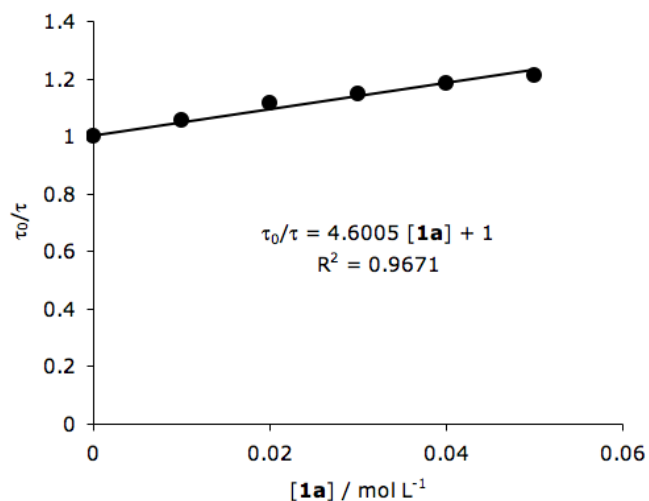


Fig. S25. Luminescence decays of $\text{Na}_3[\text{Ir}(\text{sppy})_3]$ in presence of imine **1a** in aqueous phosphate buffer at pH 8.

Table S7. Luminescence quenching of $\text{Na}_3[\text{Ir}(\text{sppy})_3]$ by imine **1e** in water at pH 8.0 (20 °C, excitation at 405 nm, emission at 510 nm). A Stern-Volmer plot is shown on the right.

$[\text{Na}_3\text{Ir}(\text{sppy})_3]$ / mol L ⁻¹	$[\mathbf{1e}]$ / mol L ⁻¹	τ / μs
2.0×10^{-5}	—	1.493
2.0×10^{-5}	2.0×10^{-4}	0.877
2.0×10^{-5}	4.0×10^{-4}	0.631
2.0×10^{-5}	6.0×10^{-4}	0.496
2.0×10^{-5}	8.0×10^{-4}	0.401
2.0×10^{-5}	1.0×10^{-3}	0.349

$k_q = 2.2 \times 10^9 \text{ L mol}^{-1} \text{ s}^{-1}$

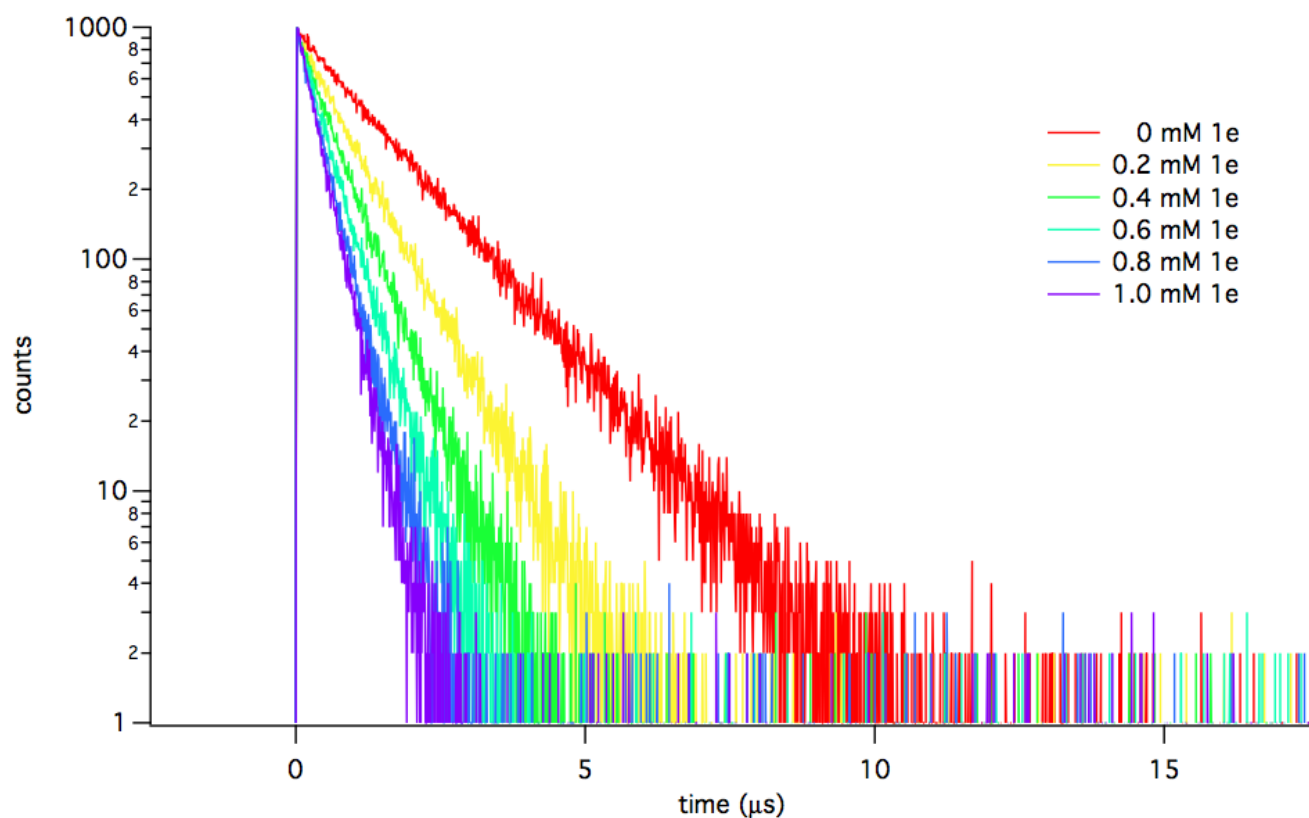
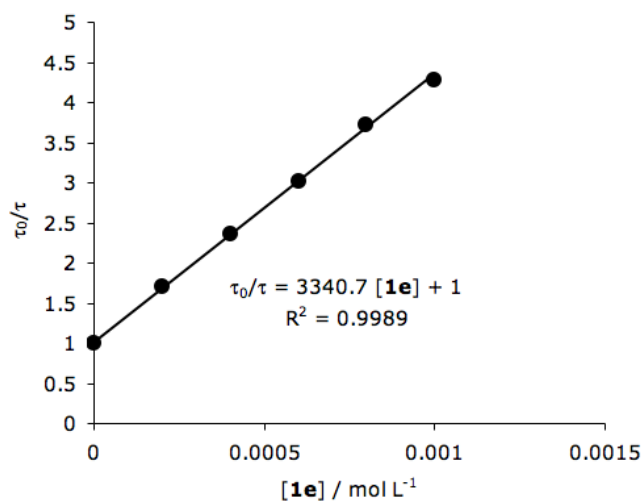


Fig. S26. Luminescence decays of $\text{Na}_3[\text{Ir}(\text{sppy})_3]$ in presence of imine **1e** in aqueous phosphate buffer at pH 8.

6) Cyclic voltammograms of imine substrates **1a** and **1e**

To determine the reduction potentials of two representative imine substrates, electrochemical measurements of **1a** and **1e** were performed in 0.5 M aqueous phosphate buffer solutions at pH 8.0. The cyclic voltammograms show that the peak reduction potentials of **1a** and **1e** are at -1.84 and -1.27 V vs. SCE respectively (Fig. S27).

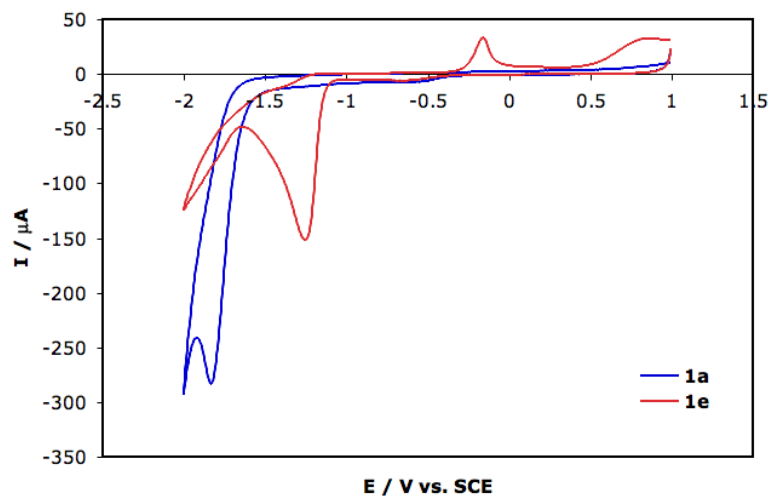


Fig. 27. Cyclic voltammograms of imine substrates **1a** and **1e**

7) References

- S1 (a) V. Köhler, Y. M. Wilson, M. Dürrenberger, D. Ghislieri, E. Churakova, T. Quinto, L. Knörr, D. Häussinger, F. Hollmann, N. J. Turner and T. R. Ward, *Nat. Chem.*, 2013, **5**, 93–99; (b) Y. Okamoto, V. Köhler and T. R. Ward, *J. Am. Chem. Soc.*, 2016, **138**, 5781–5784.
- S2 A. B. Tamayo, B. D. Alleyne, P. I. Djurovich, S. Lamansky, I. Tsyba, N. N. Ho, R. Bau and M. E. Thompson, *J. Am. Chem. Soc.*, 2003, **125**, 7377–7387.
- S3 L. C. Craig, H. Bulbrook and R. M. Hixon, *J. Am. Chem. Soc.*, 1931, **53**, 1831–1835.
- S4 G. A. Aleku, H. Man, S. P. France, F. Leipold, S. Hussain, L. Toca-Gonzalez, R. Marchington, S. Hart, J. P. Turkenburg, G. Grogan and N. J. Turner, *ACS Catal.*, 2016, **6**, 3880–3889.
- S5 A. Weller, *Z. Phys. Chem. (Leipzig)*, **1982**, *133*, 93–98.
- S6 G. J. Choi, Q. Zhu, D. C. Miller, C. J. Gu and R. R. Knowles, *Nature*, **2016**, *539*, 268–271.

- S7 C. J. Dunsmore, R. Carr, T. Fleming and N. J. Turner, *J. Am. Chem. Soc.*, 2006, **128**, 2224–2225.
- S8 (a) X. Guo and O. S. Wenger, *Angew. Chem. Int. Ed.*, 2018, **57**, 2469–2473; (b) Y. Y. Loh, K. Nagao, A. J. Hoover, D. Hesk, N. R. Rivera, S. L. Colletti, I. W. Davies and D. W. C. MacMillan, *Science*, 2017, **358**, 1182–1187.
- S9 S. Aoi, K. Mase, K. Ohkuboab and S. Fukuzumi, *Chem. Commun.*, 2015, **51**, 15145–15148.
- S10 iBonD 2.0: <http://ibond.chem.tsinghua.edu.cn>.
- S11 S. Antonello, R. Benassi, G. Gavioli, F. Taddei and F. Maran, *J. Am. Chem. Soc.*, 2002, **124**, 7529–7538.
- S12 E. L. Loechler and T. C. Hollocher, *J. Am. Chem. Soc.*, 1980, **102**, 7322–7327.
- S13 M. Montalti, A. Credi, L. Prodi and M. T. Gandolfi, *Handbook of Photochemistry, Third Edition*, CRC Press: Boca Raton, FL, 2006.